

Remote Sensing of Hail and Hail Growth in Convective Clouds

By
Robert E. Fischer

Department of Atmospheric Science
Colorado State University
Fort Collins, Colorado



**Department of
Atmospheric Science**

Paper No. 141

REMOTE SENSING OF HAIL AND
HAIL GROWTH IN CONVECTIVE CLOUDS

by
Robert E. Fischer

The research described in this report
was funded by
Contract Number NSF GA-1561
Project Director: Dr. Peter C. Sinclair

Department of Atmospheric Science
Colorado State University
Fort Collins, Colorado
June, 1969

Atmospheric Science Paper No. 141

ABSTRACT

This thesis considers the usefulness of two-wavelength radar in detecting hail in convective clouds. The basis for using two wavelengths stems from the Mie theory for the scattering of electromagnetic waves by spherical particles. In this theory the departure from Rayleigh reflection occurs for smaller hailstones at shorter wavelengths than at longer ones, enabling one to deduce hail size using reflectivity measurements at two wavelengths. The reflectivity difference is independent of the number density of the hailstones.

A severe hailstorm which occurred on 28 July 1968 was studied in detail using 88 and 34 mm wavelength radars located at New Raymer, Colorado. The storm released large amounts of hail, some as large as golf balls, over a 120 km long track. The observed reflectivities were compared with theoretical values for wet and dry hail calculated from the Mie theory. Both monodisperse and exponential size spectra were considered.

Difficulties were found in using the two-wavelength radar data. Strong attenuation of the 34 mm radar waves by cloud and precipitation particles made it nearly impossible to obtain reliable reflectivity difference measurements in the core of the storm. Compounding the problem were the lack of knowledge of the size distribution of hailstones in the cloud and the uncertainty in the accuracy of the radar reflectivity values. Measurements near the edge of the storm indicated only a small likelihood of large hail.

It is concluded that 88 and 34 mm radars would be unable to detect hail in the vital region of a well-developed storm. Such radars may be able to detect initial growth of hail before the storm matures; Soviet radar studies have shown that 100 and 32 mm radars can be successfully used in detecting initial hail growth. No data on Colorado hailstorms is currently available to verify this.

ACKNOWLEDGEMENTS

The author wishes to express gratitude to Dr. Peter C. Sinclair for his guidance and counsel during this research. Many thanks go to Dr. Robert H. Bushnell for processing much of the radar data and for many helpful discussions. Appreciation is also expressed to Professors Lewis O. Grant and Ralph H. Niemann for taking the time to read and comment on the manuscript. A sincere thanks is extended to Vincent V. Salomonson for allowing the use of a computer program which calculates the scattering amplitude coefficients. The efforts of the NCAR hail survey team were instrumental in obtaining hailfall data important to the overall success of this investigation. Marjorie Allan is to be commended for her care and attention to detail in typing the manuscript. Miss Hanae Akari performed the illustration work in a professional manner. This research was performed under the sponsorship of National Science Foundation Grant No. GA-1561.

TABLE OF CONTENTS

	Page
Abstract	ii
Acknowledgements	iii
List of Tables	vi
List of Illustrations	vii
List of Symbols	x
INTRODUCTION	1
Chapter I: BACKGROUND STUDIES	2
The radar echo top as a measure of storm intensity	2
Studies of thunderstorm reflectivity using one radar wavelength	3
Studies of hailstorms using two or more radar wavelengths	9
Chapter II: THE MIE THEORY	12
Introduction	12
Maxwell's Equations	12
Representation of the incident field in terms of the electric and magnetic potentials	16
Solution of the wave equation for the electric and magnetic potentials	17
Determination of the coefficients e_{B_ℓ} and m_{B_ℓ} and the scattered field outside the sphere	20
Computation of values of the coefficients e_{B_ℓ} and m_{B_ℓ}	22
The backscattering cross-section	23
The reflectivity of monodisperse hail size spectra	24
Reflectivity of exponential hail size spectra	32

	Page
Chapter III: RADAR EQUIPMENT AND DATA REDUCTION PROCEDURES	38
Description of the Radar Equipment	38
Reflectivity measurements at 88 mm	38
Reflectivity measurements at 34 mm	39
Radar calibration procedure	39
Calculation of observed reflectivity values	39
Chapter IV: TOPOGRAPHY AND CLIMATOLOGY OF NORTHEASTERN COLORADO	40
Chapter V: DUAL-WAVELENGTH RADAR OBSERVATIONS OF A SEVERE HAILSTORM OVER NORTHEASTERN COLORADO	42
The synoptic situation	42
Case history of the storm	42
RHI Measurements	58
Discussion	65
Chapter VI: CONCLUDING REMARKS	68
Recommendations for further research	69
REFERENCES	71

LIST OF TABLES

Table No.	Caption	Page
2.1	The components of the complex index of refraction $p - iq$ for water at various wavelengths, calculated from (2.72). The temperature is 0°C	26
3.1	M33 Radar Characteristics.	38

LIST OF ILLUSTRATIONS

Figure No.	Caption	Page
1.1	Median profiles of maximum reflectivity Z in 1957-1958 New England thunderstorms, arranged in category of most severe weather. The 51 cases of hail include 29 cases of large hail (13 mm diameter or larger) which are plotted separately. Also, the 11 tornado cases are taken from the all-inclusive rain and hail categories. The radar wavelength used was 32 mm. (Donaldson, 1961)	4
1.2	Maximum reflectivity at 107 mm wavelength versus maximum reported hail diameter for New England hailstorms in 1961. (Geotis, 1963)	6
1.3	The median vertical reflectivity profiles for Texas thunderstorms, arranged in category of most severe weather. The radar wavelength is 32 mm. (Inman and Arnold, 1961)	7
1.4	The VGI hailstorm model showing (1) the direction of motion of the cloud, (2) the hail precipitation zone, (3) the accumulation zone, and (4) the boundary of radar reflection from the large-droplet zone. (Sulakvelidze, 1966)	11
2.1	Coordinates used in solving the problem of diffraction of electromagnetic radiation by a spherical particle.	15
2.2	Reflectivity of wet hail as a function of diameter for 88 and 34 mm radar waves and, at the bottom, the difference between them in dB. (1 g m^{-3} , 0°C , $Z \text{ in mm}^6 \text{ m}^{-3}$)	27
2.3	Reflectivity of dry hail as a function of diameter for 88 and 34 mm radar waves and, at the bottom, the difference between them in dB. (1 g m^{-3} , 0°C , $Z \text{ in mm}^6 \text{ m}^{-3}$)	28
2.4	Reflectivity of wet hail as a function of diameter for 230 and 88 mm radar waves and, at the bottom, the difference between them in dB. (1 g m^{-3} , 0°C , $Z \text{ in mm}^6 \text{ m}^{-3}$)	29

Figure No.	Caption	Page
2.5	Reflectivity of dry hail as a function of diameter for 230 and 88 mm radar waves and, at the bottom, the difference between them in dB. (1 g m^{-3} , 0°C , Z in $\text{mm}^6 \text{ m}^{-3}$)	30
2.6	The difference between the reflectivities at 88 and 34 mm as a function of maximum particle diameter contained in exponential spectra of wet hailstones	35
2.7	The difference between the reflectivities at 88 and 34 mm as a function of maximum particle diameter contained in exponential spectra of wet hailstones	36
4.1	Map of the region in northeastern Colorado used in the 1968 hailstorm studies.	41
5.1	Surface chart for 0500 MDT on 28 July 1968	43
5.2	500 mb chart for 0500 MDT on 28 July 1968	44
5.3	Hailfall from the storm of 28 July 1968	46
5.4	Maximum 88 mm reflectivity of the hailstorm of 28 July 1968, measured at low elevation angles.	47
	Time (MDT) Elevation Angle	
	1934-1956 2.8°	
	1957-1959 4.2°	
	2000-2032 2.4°	
	2040 5.4°	
	2041 4.2°	
	2042-2126 3.2°	
5.5	88 mm PPI photographs of the storm of 28 July 1968. North is to the top. Scale: 1 cm = 4 km.	48
5.6	34 mm radar and visual tops of the hailstorm of 28 July 1968	56
5.7	Maximum observed 34 mm reflectivity of the hailstorm of 28 July 1968. No correction for attenuation was made.	57

Figure No.	Caption	Page
5.8	88 mm RHI photographs of the hailstorm of 28 July 1968, shortly after it reached maximum intensity. West is to the left. Scale: 1 cm = 2.8 km. The vertical scale equals the horizontal scale.	59
5.9	Reflectivities vs. height for 88 and 34 mm radar waves observed on 28 July 1968 at 2032 MDT at the distance of maximum 34 mm echo. The reflectivities are not corrected for attenuation. Azimuth: 100.13° Range: 69.6 km	63

LIST OF SYMBOLS

a	= radius of sphere
a_m	= arbitrary constant
e_{A_ℓ}, m_{A_ℓ}	= coefficients for the transmitted wave
b_m	= arbitrary constant
e_{B_ℓ}, m_{B_ℓ}	= coefficients for the diffracted wave
\vec{B}	= magnetic induction vector
c_ℓ	= arbitrary constant
c	= speed of light
d_ℓ	= arbitrary constant
\vec{D}	= electric displacement vector
D	= hailstone diameter
ΔD	= increment of hailstone diameter
e	= 2.71828182 . . .
\vec{E}	= electric field vector
E_r	= component of \vec{E} in the r direction
E_θ	= component of \vec{E} in the θ direction
E_ϕ	= component of \vec{E} in the ϕ direction
E_x	= component of \vec{E} in the x direction
E_y	= component of \vec{E} in the y direction
E_z	= component of \vec{E} in the z direction
G	= antenna gain
h	= pulse length
\vec{H}	= magnetic field vector
H_r	= component of \vec{H} in the r direction

H_θ	= component of \vec{H} in the θ direction
H_ϕ	= component of \vec{H} in the ϕ direction
H_x	= component of \vec{H} in the x direction
H_y	= component of \vec{H} in the y direction
H_z	= component of \vec{H} in the z direction
$H_{\ell+1/2}^{(1)}$	= Hankel function of the first kind of order $\ell+1/2$ = $J_{\ell+1/2} + iN_{\ell+1/2}$
i	= $\sqrt{-1}$
(i)	= a superscript referring to the incident field
\vec{j}	= electric current vector
$J_{\ell+1/2}$	= Bessel function of order $\ell+1/2$
k_1	= $\frac{1}{c}(i\varepsilon\omega - 4\pi\sigma)$
k_2	= $\frac{i\omega}{c}$
k	= wave number = $\sqrt{-k_1 k_2}$
$ K ^2$	= $\left \frac{n^2 - 1}{n^2 + 2} \right ^2$
ℓ	= integer
L	= losses in the directional coupler and cable
m	= integer
n	= complex index of refraction of sphere with respect to the surrounding medium
N_0	= a constant directly proportional to number concentration
N_D	= number of hailstones with diameters between D and $D + \Delta D$
$N_{\ell+1/2}$	= Neumann function of order $\ell+1/2$
0	= origin in rectangular and spherical coordinate system

p	= real part of the complex index of refraction
P	= an arbitrary point in the spherical coordinate system
$P_{\ell}^{(m)}$	= associated Legendre polynomial
P_r	= received power
P_t	= peak transmitted power
q	= imaginary part of the complex index of refraction
r	= radius in the spherical coordinate system
R	= a function whose independent variable is r
Re	= denotes the real part of a complex quantity
R_o	= range
(s)	= a superscript referring to the diffracted field (the field outside the sphere)
t	= time
(w)	= a superscript referring to the transmitted field (the field within the sphere)
x	= one axis of a rectangular coordinate system used in conjunction with the Mie theory
\hat{x}	= Mie size parameter
y	= one axis of a rectangular coordinate system used in conjunction with the Mie theory
Y	= a scalar function
Y_1	= electric potential
Y_2	= magnetic potential
$Y_{\ell}^{(m)}$	= a particular solution of the scalar wave equation
z	= one axis of a rectangular coordinate system used in conjunction with the Mie theory
Z	= equivalent reflectivity factor
(I)	= a superscript referring to the medium surrounding a spherical scatterer
(II)	= a superscript referring to the spherical scatterer

∇	= Del operator
∇^2	= Laplacian operator
α	= constant
β	= constant
ϵ	= dielectric constant
ϵ_0	= constant
ϵ_∞	= constant
$\zeta_\ell^{(1)}(kr)$	= $\psi_\ell(kr) - i\chi_\ell(kr) = (0.5\pi kr)^{0.5} H_{\ell+1/2}^{(1)}(kr)$
θ	= co-latitude in spherical coordinate system
θ_1	= vertical half-power beam width in radians
Θ	= a function whose independent variable is θ
Λ	= a parameter related to the rate at which the number density of particles in a specified size interval falls off exponentially according to the size of the particle
λ	= wavelength
$\Delta\lambda$	= constant
μ	= magnetic permeability
π	= 3.1415926535
ρ	= electric charge density
σ	= specific conductivity
σ_b	= backscattering cross-section
ϕ	= azimuth in spherical coordinate system
ϕ_1	= horizontal half-power beamwidth in radians
Φ	= a function whose independent variable is
$\chi_\ell(kr)$	= $-(0.5\pi kr)^{0.5} N_{\ell+1/2}(kr)$

$$\psi_{\ell}(\mathbf{kr}) = (0.5\pi\mathbf{kr})^{0.5} J_{\ell+1/2}(\mathbf{kr})$$

ω = angular frequency of radiation

INTRODUCTION

Hailstorms over the high plains are a cause of extensive crop and property damage. Since 1958, personnel at Colorado State University have been conducting field studies in northeastern Colorado in order to learn more about the physical characteristics of hailstorms and better understand the processes that take place within them. The frequent occurrence of hailstorms during the late spring and early summer makes northeastern Colorado an ideal location for field hail research. Other extensive hailstorm studies are also in progress in Canada and the Soviet Union.

One of the first objectives of hailstorm research has been to find methods of discriminating hailstorms from thunderstorms producing rain only. One of the first parameters studied was the height of the radar echo top. It has been shown by several investigators that hailers have higher average tops than nonhailers. No sharp cut-off value of height was found which separated hailers from nonhailers.

Studies of the radar reflectivities of thunderstorms were undertaken in order to obtain a more quantitative estimate of storm intensity. It was found that hailstorms generally had higher reflectivities than nonhailers, with the most highly reflective storms containing hail. High reflectivity, however, was not an absolute measure of hail. Reflectivity measurements at long wavelengths, such as 100 mm, were found to be somewhat more useful in evaluating storm intensity than those at shorter wavelengths, such as 30 mm.

As a further attempt to positively identify hailstorms, Atlas and Ludlam (1961) and personnel at the Georgian High Mountain Geophysical Institute (VGI) in the Soviet Union (Sulakvelidze, 1966, 1967; Sulakvelidze et al., 1965) have used radars operating on several wavelengths. The VGI group has reported success in identifying initial hail growth using 100 and 32 mm wavelength radars. Dual-wavelength reflectivity measurements of hailstorms were begun in the summer of 1967 in the Colorado State University research program. The objectives of the initial studies were to determine if 88 and 34 mm radars could be used to detect hail in convective clouds and to observe initial hail growth.

Chapter I
BACKGROUND STUDIES

The radar echo top height as a measure of storm intensity

From the earliest days of radar meteorology, the echo top height has been used as an indicator of the intensity of a thunderstorm. Bent (1946) suggested that echo tops of less than 5 km MSL indicated a lack of convective activity, and that the echoes observed were not from thunderstorms. Subsequent investigations, particularly those by Soviet and American researchers (Donaldson, 1965) confirmed that rain showers and thunderstorms could be distinguished from each other on the basis of echo top height. The critical height, however, was found to be far in excess of 5 km. Kotov (1960), making one of the more comprehensive attempts to distinguish thunderstorms from rain showers by use of radar, defined the echo top to be the highest vertical extent of an echo intensity corresponding to a rainfall rate of 1 mm hr^{-1} . This definition of echo top is independent of range and of radar characteristics which largely account for the variability of heights of minimum detectable echo tops. Kotov concluded that the height of the -22°C isotherm was a rather sharply defined critical height dividing shower and thunderstorm echo tops.

A number of studies have been undertaken with the objective of distinguishing hail-producing thunderstorms (hailers) from those producing rain only (nonhailers), using echo top height as the parameter. It has been found that echo tops of hailers are, in general, higher than those of nonhailers. However, the relation between echo top height and hail production is not nearly as well-defined as the distinction between thunderstorms and rain showers.

Studies of thunderstorms over the New England states (Donaldson, 1958, 1959) showed that echo tops of hailers were, in the mean, about 1.5 km higher than those of nonhailers. The chance that a storm contained hail increased as the height of the echo tops increased. Geotis (1963), making similar studies of New England thunderstorms, did not find a clear dependence of either hail size or hail duration on the echo top height. It was concluded here that

the largest hail was produced by storms with high echo tops, but all storms with high tops did not necessarily produce large hail, or even large amounts of small hail.

Studies of hailstorms occurring over the high plains of Alberta (Douglas and Hirschfeld, 1959; Douglas, 1960) again showed that hailers generally had higher echo tops than nonhailers, and that the chance of hail increased with the height of the echo tops. However, the mean echo top height of Alberta storms was about 3 km lower than those in New England. Inman and Arnold (1961) summarized their findings for Texas storms and found similar results, but here, the average echo top height for hailstorms was considerably greater than that for their New England counterparts. Results of hailstorm studies in northeastern Colorado (Schleusner and Auer, 1964) also indicated that hailers had a higher average echo top than nonhailers.

In a summary of the studies of storms in New England, Alberta, and Texas, Douglas (1963) showed that for storms with tops of 12 km, the chance of hail was almost negligible in Texas, moderate in New England, and almost certain in Alberta. The results of the studies hinted that the amount of penetration of the storm tops into the stratosphere was a better indicator of the intensity of convective activity (and of the probability of hail) than was the height of the echo top alone. Donaldson et al. (1960) showed this to be the case by comparing echo top heights with estimates of the tropopause height in the New England area. It was found that the probability of hail increased when the storm tops penetrated the tropopause. About 80 per cent of storms producing large hail (19 mm diameter or greater) exceeded the tropopause height.

Studies of thunderstorm reflectivity using one radar wavelength

The magnitude of the equivalent reflectivity factor, Z , has been found to be a good measure of the intensity of thunderstorms. Donaldson (1958, 1959, 1961) conducted extensive surveys of New England thunderstorms with 32 mm radar and found that the greatest incidence of hailfall occurred when the storm tops exceeded 15 km and the maximum reflectivity ($10 \log Z$) exceeded 50. Median profiles of New England thunderstorms (Figure 1.1) showed that tornado-producing

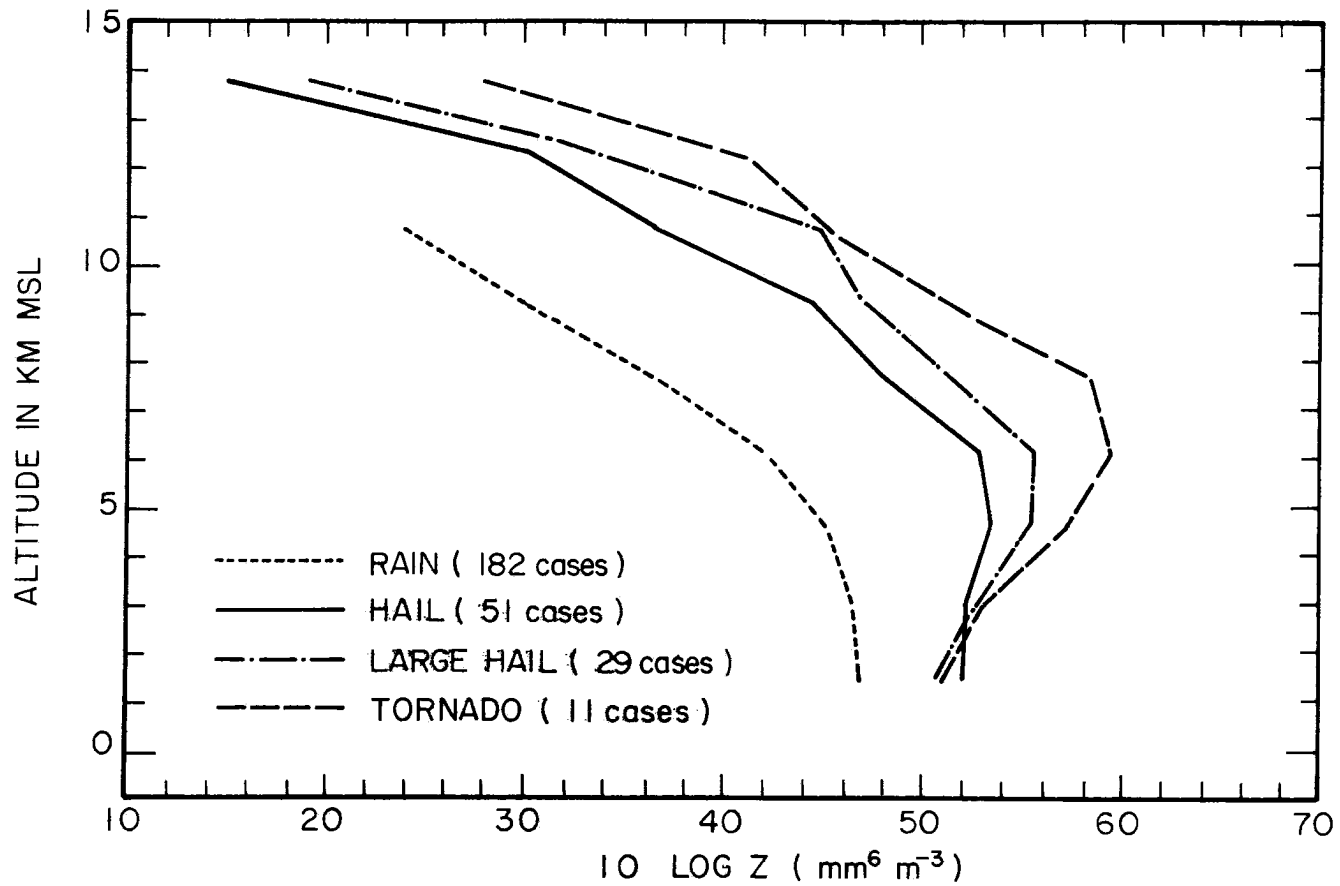


Figure 1.1. Median profiles of maximum reflectivity Z in 1957-1958 New England thunderstorms, arranged in category of most severe weather. The 51 cases of hail include 29 cases of large hail (13 mm diameter or larger) which are plotted separately. Also, the 11 tornado cases are taken from the all-inclusive rain and hail categories. The radar wavelength used was 32 mm. (Donaldson, 1961)

storms had a mean maximum reflectivity of 60 at an altitude of 6 km. One severe storm had a maximum reflectivity of 70. The maximum reflectivity zone aloft was present in the median profiles of hailstorms and tornadic storms. This maximum was more easily seen in storms producing large hail (13 mm diameter or larger) than in storms producing small hail. Donaldson found that the greatest difference between the reflectivities of hailers and nonhailers occurred at an altitude of 9 km. About 50 per cent of all hailers had reflectivities exceeding 40 at 9 km while only 20 per cent of the nonhailers exceeded the same value. Donaldson also made use of a reflectivity ratio which he defined as the ratio of the maximum observed reflectivity to the minimum core reflectivity measured at a lower altitude. Storms with both a high reflectivity ratio and a high-altitude zone of maximum reflectivity almost always contained hail. Another indicator of storm intensity used was the change in reflectivity above the freezing level. If the reflectivity increased above the freezing level the chance of hail was about 45 per cent. For storms in which the reflectivity remained constant or decreased above the freezing level the chance of hail was only 10 per cent.

Additional studies of New England storms with 107 mm radar (Geotis, 1963) showed that large hail was associated with high reflectivity (Figure 1.2). A maximum reflectivity of 55 or greater was considered to indicate the presence of hail. Reflectivity maxima aloft were not observed and the distinctions between hailers and nonhailers were made using the reflectivities at low altitudes.

Studies of Illinois thunderstorms with 32 mm radar (Wilk, 1961) showed that the highest storm reflectivities were located between heights of 3.5 and 7 km. There were no significant differences between the maximum reflectivities of hailers and nonhailers. The height of the maximum reflectivity, however, was found to be considerably greater for hailers than for nonhailers. The altitude of the highest reflectivity was most often between 5 and 6 km for hailstorms while the maxima for nonhailers were most often at or near the ground level.

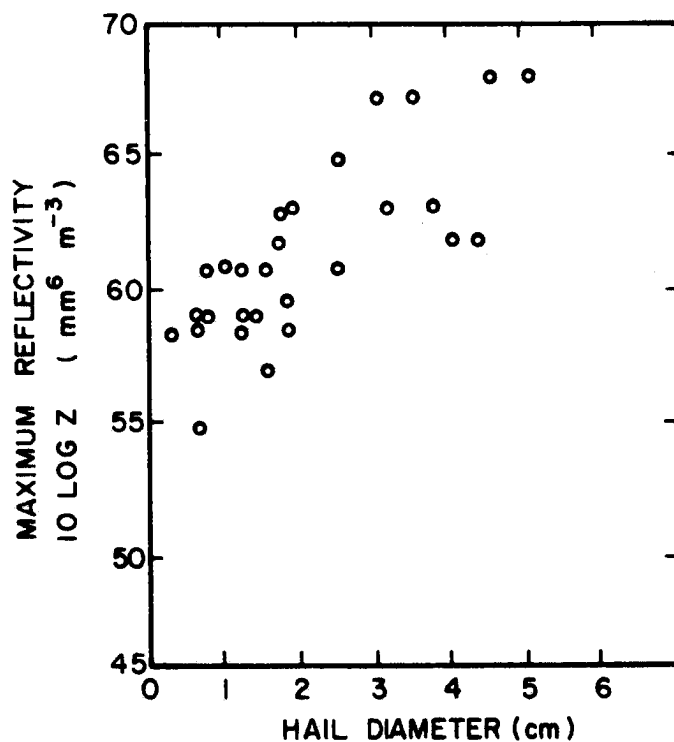


Figure 1.2. Maximum reflectivity at 107 mm wavelength versus maximum reported hail diameter for New England hailstorms in 1961. (Geotis, 1963)

Reflectivity profiles of Texas thunderstorms (Inman and Arnold, 1961) were similar to those of New England storms (Donaldson, 1961) but the maximum reflectivity aloft was not as well defined for the hail and tornado categories (Figure 1.3). Of course, distinct maxima aloft were observed in many individual cases. The highest reflectivities observed in this study were in the neighborhood of 65.

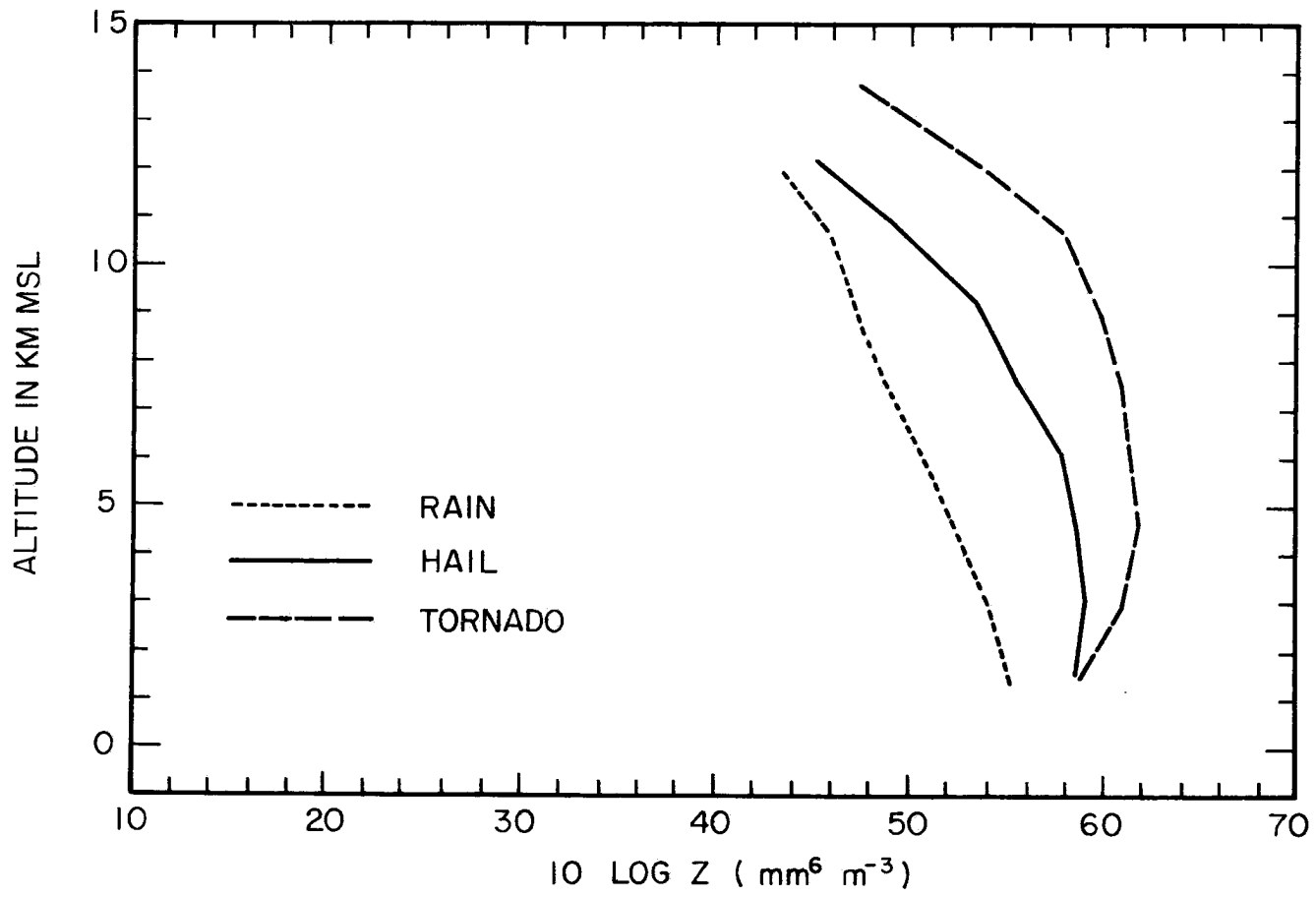


Figure 1.3. The median vertical reflectivity profiles for Texas thunderstorms, arranged in category of most severe weather. The radar wavelength is 32 mm. (Inman and Arnold, 1961)

Surveys of thunderstorms over northeastern Colorado with 32 mm radar (Schleusner and Auer, 1964) did not show any significant differences between the mean heights of the maximum reflectivity of hailers and nonhailers. Hail clouds had greater reflectivity than rain storms with the difference being greatest at a height of 9 km. Pell (1966), using 104 mm radar, observed reflectivities of 50 in two Alberta hailstorms which released hail up to golf-ball size.

Studies of Oklahoma storms with 103 mm radar (Ward et al., 1965) have shown that numerous storms which released large amounts of hail attained reflectivity values of 60 or greater. They concluded that most radar echoes having reflectivities exceeding 50 probably contained some significant hail. An intensive analysis of a severe hailstorm over central Oklahoma (Browning et al., 1968) using 103 mm radar and a dense ground reporting network showed that a reflectivity exceeding 50 was closely related to heavy rain and 10 mm hail reaching the ground. There was a good relation between regions of reflectivity exceeding 55 and golf-ball sized hail. Evidence brought forth from this survey supported the view that the regions of high reflectivity are due to the presence of large hailstones rather than high concentrations of raindrops and small spongy hailstones. A case study of an earlier storm in Oklahoma (Browning, 1965) indicated that a reflectivity of 57, measured with 103 mm radar, was associated with hail of 50 to 100 mm diameter.

Soviet researchers (Atlas, 1965) have claimed that they are able to identify hailstorms with 90 per cent confidence using 30 mm vertical reflectivity profiles. They list the following as criteria for a hailstorm:

- (1) A reflectivity of 56 or greater.
- (2) Occurrence of the maximum reflectivity at an altitude of 6 km or higher.
- (3) There exists an interval of at least 3 km where the reflectivity profile maintains a value within 10 dB of the maximum value.
- (4) The height of the radar echo top is also considered.

Studies of hailstorms using two or more radar wavelengths

Use of multi-wavelength radars in analysis of severe local storms is a relatively new idea, stemming from the Mie theory. In this theory the departure from Rayleigh reflection occurs for smaller hailstones for a shorter radar wavelength than for a longer wavelength with the result that hail size can be calculated from the difference in reflectivity. To date, the major observational work has been carried out by Atlas and Ludlam (1961) and the Georgian High Mountain Geophysical Institute (VGI) (Sulakvelidze, 1966, 1967; Sulakvelidze et al., 1965).

Observations of a severe hailstorm over southern England were carried out by Atlas and Ludlam (1961) using radars operating at 33, 47, and 100 mm wavelengths. The observed reflectivities were compared with the theoretical values for ice and water spheres. Initially, exponential spectra of the form

$$N_D = \int_D^{D + \Delta D} N_0 e^{-\Lambda D} dD \quad (1.1)$$

were assumed. Here, N_D is the number of particles with diameters between D and $D + \Delta D$. N_0 is a constant directly proportional to number density and it has the value of $4.0 \text{ m}^{-3} \text{ mm}^{-1}$. The parameter Λ , with the units of mm^{-1} , is related to the rapidity at which the number density of particles decreases as the diameter increases. It is also related to the mass density of the entire spectrum. For $\Lambda = 0$, there is an equal number of particles in each size interval of the spectrum. If Λ is positive, the number of particles in a specified size interval drops off exponentially according to the diameter of the particle. Large positive values of Λ result in low spectral mass concentrations while small positive values of Λ give high spectral mass concentrations. Atlas and Ludlam (1961) used values of Λ corresponding to mass concentrations of 4.3, 10, 20, and 40 g m^{-3} . Hailstones with diameters exceeding 60 mm were considered as being too few in number to influence the reflectivity, hence the spectra were truncated at the upper limit of $D = 60 \text{ mm}$. For such exponential distributions the reflectivity

increases rapidly as the wavelength increases, for both wet and dry hailstones. The observed reflectivities did not support the hypothesis of existence of exponential hail size spectra and it was concluded that the spectrum within the cloud was extremely narrow. In the storm studied the reflectivity reached 75.5 at 33 mm wavelength, 70.5 at 47 mm and 70 at 100 mm. These figures included an estimated correction for attenuation. Dry hail of 39 to 50 mm diameter was predicted to be within the cloud. The actual size of the hail found at the ground was in general agreement with the predicted size range, however, there was a discrepancy of a few kilometers between the predicted location of the hail and the actual location. It was concluded that the likelihood and size of hail at the ground are indicated by echo intensity aloft at 33 mm, and less sensitively at 47 mm, but not at 100 mm.

Personnel at the Georgian High Mountain Geophysical Institute (VGI) (Sulakvelidze, 1966, 1967; Sulakvelidze et al., 1965) have reported success in locating hail centers and estimating the maximum size of hail contained in thunderstorm clouds, using 32 and 100 mm radars. In their studies they assumed the existence of a monodisperse distribution of spherical hailstones with an outer covering of water. In the VGI hailstorm model the initial hail growth occurs in an accumulation zone located in the upper levels of the cloud (Figure 1.4). In the early stages of hailstorm development, only the accumulation zone is visible on radar scopes. As the precipitation process begins, both the accumulation zone and the precipitation zone can be seen. During the late stages of the storm, the accumulation zone slowly transforms into a precipitation zone. The Soviet radar studies of hailstorms have shown that the most rapid hail growth occurs in the temperature interval from -2°C to -15°C . It was also concluded that hailstones can grow from shot-size to walnut-size or larger in time intervals as short as 4 to 6 minutes. Such rapid growth requires high liquid water content within the cloud, perhaps of the order of 40 g m^{-3} . High up-draft velocities are also necessary for such a high growth rate. Rapid hail growth has also been suggested by Hitschfeld and Douglas (1961). The volume of the hail growth zone was found to vary from 10 to 15 km^3 in most cases, although it exceeded 30 km^3 in a few large storms. The vertical extent of the hail growth zone was generally 3 to

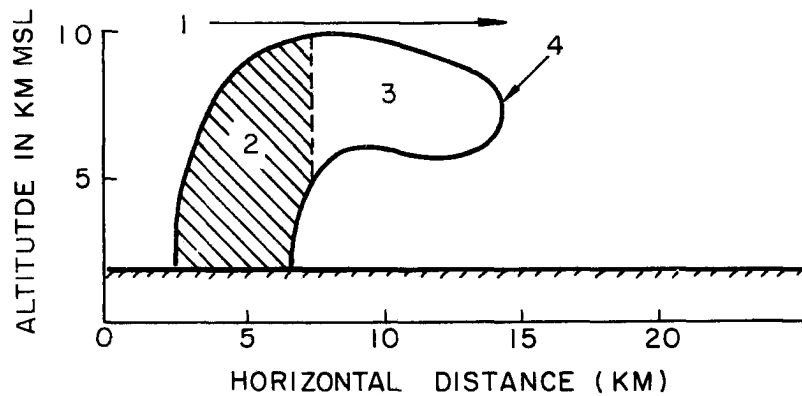


Figure 1.4. The VGI hailstorm model showing (1) the direction of motion of the cloud, (2) the hail precipitation zone, (3) the accumulation zone, and (4) the boundary of radar reflection from the large-droplet zone. (Sulakvelidze, 1966)

4 km. This is in general agreement with the results of Hitschfeld and Douglas (1961) which showed that hail growth in Alberta storms occurred between heights of 4 and 8 km. Calculations by the VGI scientists, using the distribution and number of hailstones falling on a unit area from a cloud whose accumulation zone volume was known, showed that the number concentration of hailstones contained in the cloud varied from 0.1 to 10 m^{-3} . The VGI people have claimed that an average number density of 1 m^{-3} is sufficiently accurate for deducing the size of the hailstones from the reflectivity of the accumulation zone (Goyer, 1967). The Soviet group claims that the hail as measured at the ground is within 35 per cent of the size calculated from the radar measurements, after correction for melting.

Chapter II

THE MIE THEORY

Introduction

In order to calculate the reflectivity of a specified distribution of hailstones illuminated by radar waves, the theory of scattering of electromagnetic radiation by spherical particles is usually employed. This theory was first developed by Mie (1908) and leads to a solution of Maxwell's equations which describes the electromagnetic field at any point in space, generated when a plane monochromatic wave strikes the surface of a conducting sphere of uniform composition differing from that of the surrounding medium. This field is described as a superposition of two secondary fields. Spherical coordinates are introduced and Maxwell's equations together with the prescribed boundary conditions are separated into a set of three ordinary differential equations. These equations are typically solved for the secondary fields using standard methods. The unknown coefficients are then determined by applying the boundary conditions. In this section, the development of the Mie theory is first briefly summarized and is then used to show how the reflectivity of monodisperse and exponential hail size spectra can be calculated.

Maxwell's Equations

The incident radiation is assumed to be in the form of a plane, linearly polarized monochromatic wave which is diffracted by a conducting sphere of radius which is embedded in a homogeneous, isotropic dielectric medium. Both the sphere and the surrounding medium are assumed to be nonmagnetic. The incident radiation is assumed to have the time dependence

$$e^{-i\omega t} = \cos \omega t - i \sin \omega t . \quad (2.1)$$

For a homogeneous isotropic medium, Maxwell's equations have the following form when using Gaussian units:

$$\nabla \times \vec{H} = \frac{4\pi\vec{j}}{c} + \frac{1}{c} \frac{d\vec{D}}{dt}, \quad (2.2)$$

$$\nabla \times \vec{E} = -\frac{1}{c} \frac{d\vec{B}}{dt}, \quad (2.3)$$

$$\nabla \cdot \vec{D} = 4\pi\rho, \quad (2.4)$$

$$\nabla \cdot \vec{B} = 0. \quad (2.5)$$

These equations connect the five basic quantities \vec{E} , \vec{H} , \vec{B} , \vec{D} , and \vec{j} . To allow a unique determination of the field vectors from a given distribution of fields and charges, these equations must be supplemented by relations which describe the behavior of substances when under the influence of an electromagnetic field. These relations are known as the "material equations." If the material particles are at rest or in very slow motion relative to each other, and if the material is isotropic, the material equations assume the form:

$$\vec{j} = \sigma\vec{E}, \quad (2.6)$$

$$\vec{D} = \epsilon\vec{E}, \quad (2.7)$$

$$\vec{B} = \mu\vec{H}. \quad (2.8)$$

The following assumptions are made which are true for all homogeneous, isotropic, dielectric materials:

- (1) The quantities σ , ϵ , and μ are time-independent.
- (2) The magnetic permeabilities of the sphere and surrounding medium are equal to 1.
- (3) The scatterers are not charged.
- (4) The electric and magnetic fields vary with $e^{-i\omega t}$.

Using the material equations and the assumptions given above, Maxwell's equations (Eqs. 2.2-2.5) may be written as:

$$\nabla \times \vec{H} = -k_1\vec{E}, \quad (2.9)$$

$$\nabla \times \vec{E} = k_2\vec{H}. \quad (2.10)$$

$$\nabla \cdot \vec{H} = 0, \quad (2.11)$$

$$\nabla \cdot \vec{E} = 0. \quad (2.12)$$

With the aid of the triple vector product identity the equations 2.9-2.12 can be combined into the relations

$$[\nabla^2 + k^2]\vec{E} = 0, \quad (2.13)$$

$$[\nabla^2 + k^2]\vec{H} = 0, \quad (2.14)$$

where $k^2 = -k_1 k_2$. If \vec{E} or \vec{H} in Eqs. 2.14 or 2.15 is replaced by the scalar Y then one has the scalar wave equation

$$[\nabla^2 + k^2]Y = 0. \quad (2.15)$$

This equation will be referred to later on in the discussion.

Quantities which refer to the medium surrounding the sphere will be denoted by a superscript (I) and those referring to the sphere itself by a superscript (II). In a rectangular coordinate system with the center of the sphere at the origin, the z-direction is taken to be the direction of propagation of the incident radiation. The x-direction is defined to be that of the electric vector. Figure 2.1 shows rectangular and spherical coordinates employed in solving the scattering problem. In the following discussion, the superscript (i) refers to the incident field while the superscripts (s) and (w) refer to the scattered fields outside and within the sphere respectively. To simplify the calculations, the amplitude of the electric vector of the incident radiation is normalized to a value of 1.

The electromagnetic field must satisfy certain prescribed boundary conditions as well as Maxwell's equations. For example, Maxwell's equations must be satisfied at the boundary between the sphere and the surrounding medium. In addition, the scattered field must behave regularly at the origin and at infinite distances from the center of the sphere. It is specified that the tangential

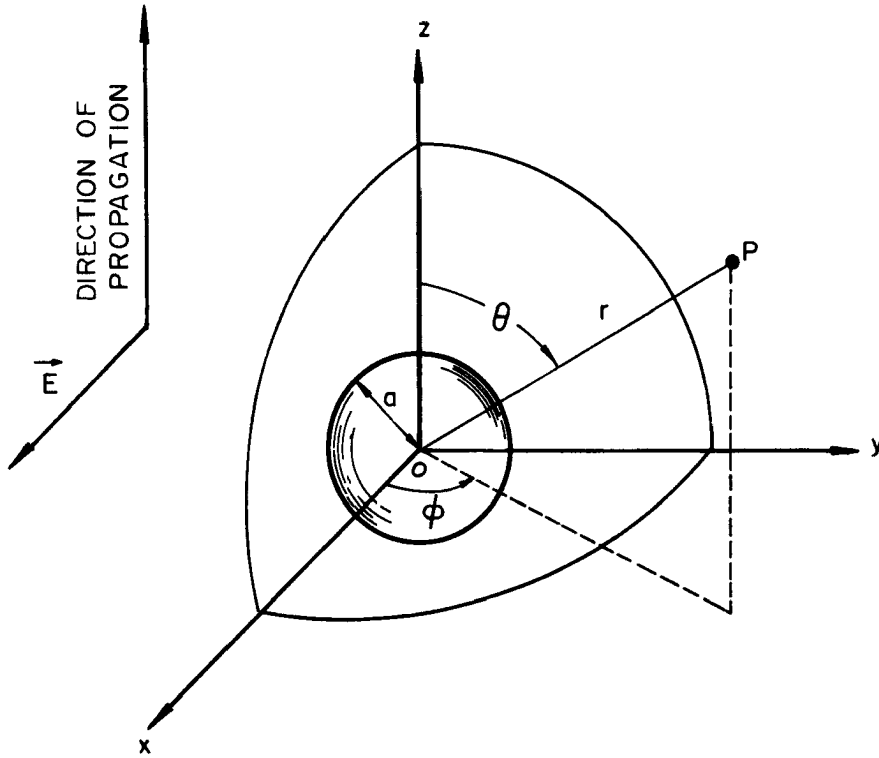


Figure 2.1. Coordinates used in solving the problem of diffraction of electromagnetic radiation by a spherical particle.

components of \vec{E} and \vec{H} must be continuous across the surface of the sphere. The radial components of $\epsilon\vec{E}$ and \vec{H} must also be continuous over this surface. All six components of the field vectors must have the same time dependence $e^{-i\omega t}$ since the scattered radiation must have the same frequency as the incident radiation. The total electric field can be expressed as

$$\vec{E} = \vec{E}^{(i)} + \vec{E}^{(s)} \quad (2.16a)$$

outside the sphere, and

$$\vec{E} = \vec{E}^{(w)} \quad (2.16b)$$

within the sphere.

The magnetic field can be described similarly.

It is useful to introduce spherical coordinates in solving this problem. Using the transformation equations relating the rectangular and spherical coordinate systems and the expression for the curl in spherical coordinates, Maxwell's equations (Eqs. 2.13 and 2.14) can be written as:

$$-k_1 E_r = \frac{1}{r^2 \sin\theta} \left[\frac{\partial}{\partial\theta}(rH_\phi \sin\theta) - \frac{\partial}{\partial\phi}(rH_\theta) \right], \quad (2.17)$$

$$-k_1 E_\theta = \frac{1}{r \sin\theta} \left[\frac{\partial Hr}{\partial\phi} - \frac{\partial}{\partial r}(rH_\phi \sin\theta) \right], \quad (2.18)$$

$$-k_1 E_\phi = \frac{1}{r} \left[\frac{\partial}{\partial r}(rH_\theta) - \frac{\partial Hr}{\partial\theta} \right], \quad (2.19)$$

$$k_2 H_r = -\frac{1}{r^2 \sin\theta} \left[\frac{\partial}{\partial\theta}(rE_\phi \sin\theta) - \frac{\partial}{\partial\phi}(rE_\theta) \right], \quad (2.20)$$

$$k_2 H_\theta = \frac{1}{r \sin\theta} \left[\frac{\partial E_r}{\partial\phi} - \frac{\partial}{\partial r}(rE_\phi \sin\theta) \right], \quad (2.21)$$

$$k_2 H_\phi = \frac{1}{r} \left[\frac{\partial}{\partial r}(rE_\theta) - \frac{\partial E_r}{\partial\theta} \right]. \quad (2.22)$$

Representation of the incident field in terms of the electric and magnetic potentials

The six components of the incident field can be expressed in terms of two unknown functions which are known as the electric and magnetic potentials. These functions are sometimes called Debye's potentials. The incident field can be represented as a superposition of two types of waves. One wave will have a vanishing magnetic field in the radial direction and will be termed the electric wave. The wave with a vanishing electric field in the radial direction will be termed the magnetic wave. It can be shown (Cf. Born and Wolf, 1965; Shifrin, 1951) that the electric wave can be expressed in terms of the electric potential Y_1 and the magnetic wave in terms of the magnetic potential Y_2 . The total field is obtained by adding together the corresponding components of the electric and magnetic waves:

$$E_r = \left(\frac{\partial^2}{\partial r^2} + k^2 \right) (rY_1), \quad (2.23)$$

$$E_\theta = \frac{1}{r} \frac{\partial^2}{\partial r \partial \theta} (rY_1) + \frac{k_2}{r \sin \theta} \frac{\partial}{\partial \phi} (rY_2), \quad (2.24)$$

$$E_\phi = \frac{1}{r \sin \theta} \frac{\partial^2}{\partial r \partial \phi} (rY_1) - \frac{k_2}{r} \frac{\partial}{\partial \theta} (rY_2) \quad (2.25)$$

$$H_r = \left(\frac{\partial^2}{\partial r^2} + k^2 \right) (rY_2), \quad (2.26)$$

$$H_\theta = \frac{1}{r} \frac{\partial^2}{\partial r \partial \theta} (rY_2) - \frac{k_1}{r \sin \theta} \frac{\partial}{\partial \phi} (rY_1), \quad (2.27)$$

$$H_\phi = \frac{1}{r \sin \theta} \frac{\partial^2}{\partial r \partial \phi} (rY_2) + \frac{k_1}{r} \frac{\partial}{\partial \theta} (rY_1). \quad (2.28)$$

The boundary conditions specify that the θ and ϕ components of \vec{E} and \vec{H} must be continuous across the surface of the sphere. The quantities $k_1 rY_1$, $k_2 rY_2$, $\frac{\partial}{\partial r}(rY_1)$ and $\frac{\partial}{\partial r}(rY_2)$ must also be continuous across the surface. The scattering problem is reduced to that of finding two independent solutions of the wave equation with the prescribed boundary conditions.

Solution of the wave equation for the electric and magnetic potentials

It can be shown (Born and Wolf, 1965) that the electric and magnetic potentials are solutions of the wave equation

$$[\nabla^2 + k^2]Y_i = 0 \quad (i = 1,2). \quad (2.29)$$

The solutions will be represented as series expansions with undetermined coefficients. Each term of the expansions represents a particular integral. The desired solutions are of the form

$$Y(r, \theta, \phi) = R(r)\Theta(\theta)\Phi(\phi). \quad (2.30)$$

Using the method of separation of variables, the wave equation written in spherical coordinates can be reduced to a set of three ordinary differential equations

$$\frac{d^2\phi}{d\phi^2} = -\beta\phi, \quad (2.31)$$

$$\frac{1}{\sin\theta} \frac{d}{d\theta} \left(\sin\theta \frac{d\theta}{d\theta} \right) + \left(\alpha - \frac{\beta}{\sin^2\theta} \right) \theta = 0, \quad (2.32)$$

$$\frac{d^2}{dr^2}(rR) = \left[k^2 - \frac{\alpha}{r^2} \right] (rR) = 0. \quad (2.33)$$

where α and β are constants. Equations 2.32 and 2.33 can be transformed into Legendre and Bessel equations respectively by using appropriate changes of variable. These equations are then typically solved using standard series solution methods. Since the electromagnetic field is a single-valued function of position, the electric and magnetic potentials must also be single-valued functions of position. A particular integral $Y_\ell^{(m)}$ of the wave equation is obtained by multiplying together the single-valued solutions of (2.31) and of the Legendre and Bessel equations derived from (2.32) and (2.33) respectively:

$$Y_\ell^{(m)} = \frac{1}{r} [c_\ell \psi_\ell(kr) + d_\ell \chi_\ell(kr)] [P_\ell^{(m)}(\cos\theta)] [a_m \cos m\phi + b_m \sin m\phi]. \quad (2.34)$$

The quantities a_m , b_m , c_ℓ , and d_ℓ are arbitrary constants. The general solution of the wave equation can then be written as

$$Y = \sum_{\ell=0}^{\infty} \sum_{m=-\ell}^{\ell} Y_\ell^{(m)}. \quad (2.35)$$

The functions $\psi_\ell(kr)$ and $\chi_\ell(kr)$ are defined as:

$$\psi_\ell(kr) = \sqrt{\frac{\pi kr}{2}} J_{\ell+1/2}(kr), \quad (2.36)$$

$$\chi_\ell(kr) = -\sqrt{\frac{\pi kr}{2}} N_{\ell+1/2}(kr). \quad (2.37)$$

The functions $P_\ell^{(m)}(\cos\theta)$ are the associated Legendre polynomials in $\cos\theta$.

The components of the incident wave can be expressed as:

$$E_x^{(i)} = e^{ik^{(I)}z}, \quad (2.38)$$

$$H_y^{(i)} = \frac{ik^{(I)}}{k_2^{(I)}} e^{ik^{(I)}z}, \quad (2.39)$$

$$E_y^{(i)} = E_z^{(i)} = H_x^{(i)} = H_z^{(i)} = 0. \quad (2.40)$$

Using the expressions of the incident wave in spherical coordinates along with Eqs. 2.26-2.31 and appropriate mathematical identities (Born and Wolf, 1965), it is possible to find expressions for the electric and magnetic potentials of the incident radiation:

$$Y_1^{(i)} = \frac{1}{rk^{(I)2}} \sum_{\ell=1}^{\infty} i^{\ell-1} \frac{2\ell+1}{\ell(\ell+1)} \psi_{\ell}(k^{(I)}r) P_{\ell}^{(1)}(\cos\theta) \cos\phi, \quad (2.41)$$

$$Y_2^{(i)} = \frac{1}{rk^{(I)2}} \sum_{\ell=1}^{\infty} i^{\ell} \frac{K^{(I)}}{k_2^{(I)}} \frac{2\ell+1}{\ell(\ell+1)} \psi_{\ell}(k^{(I)}r) P_{\ell}^{(1)}(\cos\theta) \sin\phi. \quad (2.42)$$

According to (2.41) and (2.42) the boundary conditions can be satisfied only if $m = 1$ and if $a_1 = 0$ for the magnetic potential and $b_1 = 0$ for the electric potential. For the case of the incident wave, the constants c_{ℓ} and d_{ℓ} take on the values 1 and 0 respectively.

For representation of the scattered field within the sphere, only the functions $\psi_{\ell}(k^{(II)}r)$ are appropriate since they behave regularly at the origin. The functions $\chi_{\ell}(k^{(II)}r)$ are unsatisfactory since they have singularities at the origin where they become infinite. One can then write trial solutions for the electric and magnetic potentials of the field within the sphere

$$Y_1^{(w)} = \frac{1}{rk^{(II)2}} \sum_{\ell=1}^{\infty} e_{A_{\ell}} \psi_{\ell}(k^{(II)}r) P_{\ell}^{(1)}(\cos\theta) \cos\phi, \quad (2.43)$$

$$Y_2^{(w)} = \frac{i}{rk^{(II)} k_2^{(II)}} \sum_{\ell=1}^{\infty} m_{A_\ell} \psi_\ell(k^{(II)} r) P_\ell^{(1)}(\cos \theta) \sin \phi, \quad (2.44)$$

where ${}^e A_\ell$ and ${}^m A_\ell$ are undetermined coefficients.

To describe the scattered field outside the sphere, the function

$$\left[\frac{\pi k^{(I)} r}{2} \right]^{1/2} H_{\ell+1/2}^{(1)}(k^{(I)} r) = \zeta_\ell^{(1)}(k^{(I)} r) = \psi_\ell(k^{(I)} r) - i\chi_\ell(k^{(I)} r) \quad (2.45)$$

is appropriate, since for large values of $k^{(I)} r$ the function $\zeta_\ell^{(1)}(k^{(I)} r)$ behaves as $e^{ik^{(I)} r}$ and $\zeta_\ell^{(1)}(k^{(I)} r)/r$ as $e^{ik^{(I)} r}/r$. Thus, at large distances from the sphere, the scattered wave is spherical with its center at the origin. Trial solutions for the potentials of the scattered field outside the sphere can be written as:

$$Y_1^{(s)} = \frac{1}{rk^{(I)2}} \sum_{\ell=1}^{\infty} e_{B_\ell} \zeta_\ell^{(1)}(k^{(I)} r) P_\ell^{(1)}(\cos \theta) \cos \phi, \quad (2.46)$$

$$Y_2^{(s)} = \frac{i}{rk^{(I)} k_2^{(I)}} \sum_{\ell=1}^{\infty} m_{B_\ell} \zeta_\ell^{(1)}(k^{(I)} r) P_\ell^{(1)}(\cos \theta) \sin \phi. \quad (2.47)$$

The quantities ${}^e B_\ell$ and ${}^m B_\ell$ are undetermined coefficients.

Determination of the coefficients ${}^e B_\ell$ and ${}^m B_\ell$ and the scattered field outside the sphere

The boundary conditions of the problem may be stated precisely as follows:

$$\frac{\partial}{\partial r} [rY_1^{(i)} + rY_1^{(s)}]_{r=a} = \frac{\partial}{\partial r} [rY_1^{(w)}]_{r=a}, \quad (2.48)$$

$$\frac{\partial}{\partial r} [rY_2^{(i)} + rY_2^{(s)}]_{r=a} = \frac{\partial}{\partial r} [rY_2^{(w)}]_{r=a}, \quad (2.49)$$

$$k_1^{(I)} [rY_1^{(i)} + rY_1^{(s)}]_{r=a} = k_1^{(II)} [rY_1^{(w)}]_{r=a} , \quad (2.50)$$

$$k_2^{(I)} [rY_2^{(i)} + rY_2^{(s)}]_{r=a} = k_2^{(II)} [rY_2^{(w)}]_{r=a} . \quad (2.51)$$

Substitution of the expressions (2.43), (2.44), (2.46) and (2.47) into the boundary conditions (2.48-2.51) results in four linear relations between the coefficients e_{A_ℓ} , m_{A_ℓ} , e_{B_ℓ} , and m_{B_ℓ} . We are interested in determining the coefficients e_{B_ℓ} and m_{B_ℓ} which characterize the scattered wave outside the sphere. Expressions for e_{B_ℓ} and m_{B_ℓ} can be obtained by eliminating e_{A_ℓ} and m_{A_ℓ} from the linear relations between the coefficients, resulting in

$$e_{B_\ell} = \frac{i^{\ell+1} [2\ell+1]}{\ell[\ell+1]} \frac{n\psi'_\ell(\hat{x}) \psi_\ell(n\hat{x}) - \psi_\ell(\hat{x}) \psi'_\ell(n\hat{x})}{n\zeta_\ell^{(1)'}(\hat{x}) \psi_\ell(n\hat{x}) - \zeta_\ell^{(1)'}(\hat{x}) \psi'_\ell(n\hat{x})} , \quad (2.52)$$

$$m_{B_\ell} = \frac{i^{\ell+1} [2\ell+1]}{\ell[\ell+1]} \frac{n\psi_\ell(\hat{x}) \psi'_\ell(n\hat{x}) - \psi'_\ell(\hat{x}) \psi_\ell(n\hat{x})}{n\zeta_\ell^{(1)'}(\hat{x}) \psi'_\ell(n\hat{x}) - \zeta_\ell^{(1)'}(\hat{x}) \psi_\ell(n\hat{x})} , \quad (2.53)$$

where n is the complex index of refraction and \hat{x} is the Mie size parameter. The quantities n and \hat{x} are defined by the following:

$$n = \frac{k^{(II)} k_2^{(I)}}{k^{(I)} k_2^{(II)}} = \left[\frac{\epsilon^{(II)}}{\epsilon^{(I)}} + \frac{4i\pi\sigma}{\epsilon^{(I)} \omega} \right]^{1/2} , \quad (2.54)$$

$$\hat{x} = \frac{2\pi a}{\lambda^{(I)}} . \quad (2.55)$$

The components of the scattered field are obtained by substituting from (2.46-2.47) into (2.23-2.28) giving the expressions:

$$E_r^{(s)} = \frac{1}{k^{(I)2}} \frac{\cos \phi}{r^2} \sum_{\ell=1}^{\infty} \ell(\ell+1) e_{B_\ell} \zeta_\ell^{(1)}(k^{(I)} r) P_\ell^{(1)}(\cos \theta) , \quad (2.56)$$

$$E_{\theta}^{(s)} = -\frac{1}{k^{(I)}} \frac{\cos \phi}{r} \sum_{\ell=1}^{\infty} [e_{B_{\ell} \zeta_{\ell}}^{(1)'} (k^{(I)} r) P_{\ell}^{(1)'} (\cos \theta) \sin \theta - i m_{B_{\ell} \zeta_{\ell}}^{(1)} (k^{(I)} r) P_{\ell}^{(1)} (\cos \theta) \frac{1}{\sin \theta}], \quad (2.57)$$

$$E_{\phi}^{(s)} = -\frac{1}{k^{(I)}} \frac{\sin \phi}{r} \sum_{\ell=1}^{\infty} [e_{B_{\ell} \zeta_{\ell}}^{(1)'} (k^{(I)} r) P_{\ell}^{(1)} (\cos \theta) \frac{1}{\sin \theta} - i m_{B_{\ell} \zeta_{\ell}}^{(1)} (k^{(I)} r) P_{\ell}^{(1)'} (\cos \theta) \sin \theta], \quad (2.58)$$

$$H_r^{(s)} = \frac{i}{k^{(I)} k_2^{(I)}} \frac{\sin \phi}{r^2} \sum_{\ell=1}^{\infty} \ell(\ell+1) m_{B_{\ell} \zeta_{\ell}}^{(1)} (k^{(I)} r) P_{\ell}^{(1)} (\cos \theta), \quad (2.59)$$

$$H_{\theta}^{(s)} = -\frac{1}{k_2^{(I)}} \frac{\sin \phi}{r} \sum_{\ell=1}^{\infty} [e_{B_{\ell} \zeta_{\ell}}^{(1)} (k^{(I)} r) P_{\ell}^{(1)} (\cos \theta) \frac{1}{\sin \theta} + i m_{B_{\ell} \zeta_{\ell}}^{(1)'} (k^{(I)} r) P_{\ell}^{(1)'} (\cos \theta) \sin \theta], \quad (2.61)$$

$$H_{\phi}^{(s)} = \frac{1}{k_2^{(I)}} \frac{\cos \phi}{r} \sum_{\ell=1}^{\infty} [e_{B_{\ell} \zeta_{\ell}}^{(1)} (k^{(I)} r) P_{\ell}^{(1)'} (\cos \theta) \sin \theta + i m_{B_{\ell} \zeta_{\ell}}^{(1)'} (k^{(I)} r) P_{\ell}^{(1)} (\cos \theta) \frac{1}{\sin \theta}].$$

The addition of a prime to the functions ψ_{ℓ} , $\zeta_{\ell}^{(1)}$, and $P_{\ell}^{(1)}$ denotes differentiation with respect to their arguments. The formulas (2.56) through (2.61) represent the formal solution to the problem.

Computation of values of the coefficients $e_{B_{\ell}}$ and $m_{B_{\ell}}$

To calculate the values of the scattering amplitude coefficients, the method of Deirmendjian and Clasen (1962) was used. All of the

necessary functions are generated by appropriate recursion formulas. The coefficients e_{B_ℓ} and m_{B_ℓ} can be expressed as functions of n and \hat{x} , in the form:

$$e_{B_\ell}(n, \hat{x}) = \frac{[\frac{\ell}{n} + \frac{\ell}{\hat{x}}] \text{Re}(w_\ell) - \text{Re}(w_{\ell-1})}{w_\ell [\frac{\ell}{n} + \frac{\ell}{\hat{x}}] - w_{\ell-1}}, \quad (2.62)$$

$$m_{B_\ell}(n, \hat{x}) = \frac{[nA_\ell + \frac{\ell}{\hat{x}}] \text{Re}[w_\ell] - \text{Re}(w_{\ell-1})}{w_\ell [nA_\ell + \frac{\ell}{\hat{x}}] - w_{\ell-1}}. \quad (2.63)$$

The function w_ℓ is connected with half-order Bessel functions and has the recursion form

$$w_\ell(\hat{x}) = \frac{2\ell - 1}{x} w_{\ell-1} - w_{\ell-2} \quad (2.64)$$

with the functions w_0 and w_{-1} being given by

$$w_0 = \sin \hat{x} + i \cos \hat{x}, \quad (2.65)$$

$$w_{-1} = \cos \hat{x} - i \sin \hat{x}. \quad (2.66)$$

The recursion relation for $A_\ell(n\hat{x})$ is

$$A_\ell(n\hat{x}) = -\frac{\ell}{n\hat{x}} + \frac{1}{\frac{\ell}{n\hat{x}} - A_{\ell-1}(n\hat{x})} \quad (2.67)$$

where $A_0(n\hat{x})$ is given by

$$A_0(n\hat{x}) = \frac{\sin p\hat{x} \cos p\hat{x} + i \sinh q\hat{x} \cosh q\hat{x}}{\sin^2 p\hat{x} + \sinh^2 p\hat{x}} \quad (2.68)$$

where $n = p - iq$.

The back-scattering cross-section

Using expressions for the components of the scattered field and the scattering amplitude coefficients, it is possible to find an expression for the back-scattering cross-section of a spherical particle. The details of this derivation may be found in Aden (1952).

Battan (1959) defines the back-scattering cross-section as "the area intercepting that amount of power, which, if scattered isotropically, would return to the receiver an amount of power equal to that actually received." Another definition of the back-scattering cross-section is that it is "the area which, when multiplied by the incident intensity, gives the total power radiated by an isotropic source which radiates the same power in the backward direction as the scatterer." In mathematical form, the back-scattering cross-section σ_b is defined as

$$\sigma_b = \frac{\pi a^2}{\hat{x}^2} \left| \sum_{\ell=1}^{\infty} (-1)^\ell (2\ell+1) (e_{B_\ell} - m_{B_\ell}) \right|^2. \quad (2.69)$$

A FORTRAN IV program written for the CDC-6400 computer using the formulas (2.62) through (2.69) was used to calculate the functions e_{B_ℓ} and m_{B_ℓ} (Salomonson, 1968). The program was modified to calculate σ_b and the reflectivities of monodisperse and exponential spectra of wet and dry hailstones. In a check run of the modified program, the values of σ_b for ice spheres at a wavelength of 32 mm agreed closely with those published by Herman and Battan (1961a) and Stephens (1961). The developers of this routine claim an accuracy of at least five decimal places in the functions e_{B_ℓ} and m_{B_ℓ} .

The reflectivity of monodisperse hail size spectra

The method for computing the reflectivity of hailstones incorporates the routine for calculating σ_b . In making these calculations, the following assumptions were made:

- (1) The particles are spherical and of uniform composition.
- (2) The particles are evenly distributed throughout the entire volume illuminated by the radar beam.
- (3) The effects of multiple scattering, if any, are neglected. In a monodisperse spectrum, all the particles are of the same diameter.

Battan (1959) gives the following formula for the backscattering cross-section of a spherical particle:

$$\sigma_b = \frac{64\pi^5 |K|^2 a^6}{\lambda^4} . \quad (2.70)$$

This equation is sometimes called the "Rayleigh approximation" to the backscattering cross-section. For a number of particles in a unit volume and defining the sum of the sixth powers of the particle diameters per unit volume as the equivalent reflectivity factor Z , (2.70) becomes:

$$Z = \frac{\lambda^4 \sum_i \sigma_{b_i}}{\pi^5 |K|^2} . \quad (2.71)$$

The formula (2.71) is the one used in computing the hailstone reflectivities, using the value of σ_b obtained from (2.69). Appropriate values of $|K|^2$ are given in Battan (1959).

In performing the actual calculations, a mass density of 1 g m^{-3} was assumed. The densities of water and ice were assumed to be 1 g cm^{-3} . Wet hailstones (ice spheres with an outer covering of water) were assumed to reflect like all-water spheres at the same temperature. It has been shown by several investigators (Herman and Battan, 1961b; Atlas et al., 1960) that ice spheres covered by a thin film of water reflect almost like all-water spheres. In the radar studies of a severe hailstorm to be discussed later, the hail was assumed to grow in a supercooled water regime at temperatures between 0°C and -20°C . In such a growth regime it is not unreasonable to believe that growing hailstones will have an outer coating of water.

Computations were done for a particle temperature of 0°C . Values for the complex index of refraction of water were calculated from the Debye equation (Kerr, 1951):

$$n = \left[\frac{\epsilon_0 - \epsilon_\infty}{1 + \frac{i\Delta\lambda}{\lambda}} + \epsilon_\infty \right]^{1/2} . \quad (2.72)$$

For water at a temperature of 0°C, the dimensionless constants ϵ_0 and ϵ_∞ take on the values of 88 and 5.5 respectively. The constant $\Delta\lambda$ has the value of 35.9 mm. Table 2.1 shows the components of the complex index of refraction of water at various wavelengths.

Table 2.1. The components of the complex index of refraction $p - iq$ for water at various wavelengths, calculated from (2.72). The temperature is 0°C.

λ (mm)	p	q
34	7.25	2.84
88	8.88	1.62
162	9.22	0.94
230	9.30	0.68

The complex index of refraction of ice at 0°C is independent of λ with the appropriate values of p and q being 1.78 and .0024 respectively.

Calculations of reflectivity were performed for monodisperse distributions of wet and dry hailstones for wavelengths of 34, 88, 162, and 230 mm. The results for 34, 88, and 230 mm are presented in Figures 2.2-2.5. Each figure shows the reflectivity of 1 g m^{-3} of water or ice at two wavelengths. Also shown is the difference between the reflectivities in decibels. Note that the reflectivity difference is independent of the concentration of the particles, making it theoretically possible to determine the largest likely hail size contained in a particular cloud volume by making simultaneous reflectivity measurements at two wavelengths.

Figure 2.2 shows the reflectivity of wet hailstones at 88 and 34 mm wavelengths. The functions are oscillatory in nature. As the particle diameter increases to values much greater than the wavelength, the Mie backscattering cross-section approaches the geometrical cross-section which is simply the cross-sectional area of the particle. Note that the reflectivity difference increases rapidly between diameters of 6.7 mm and 18.4 mm. This is of paramount importance because it makes possible the detection of initial hailstone growth.

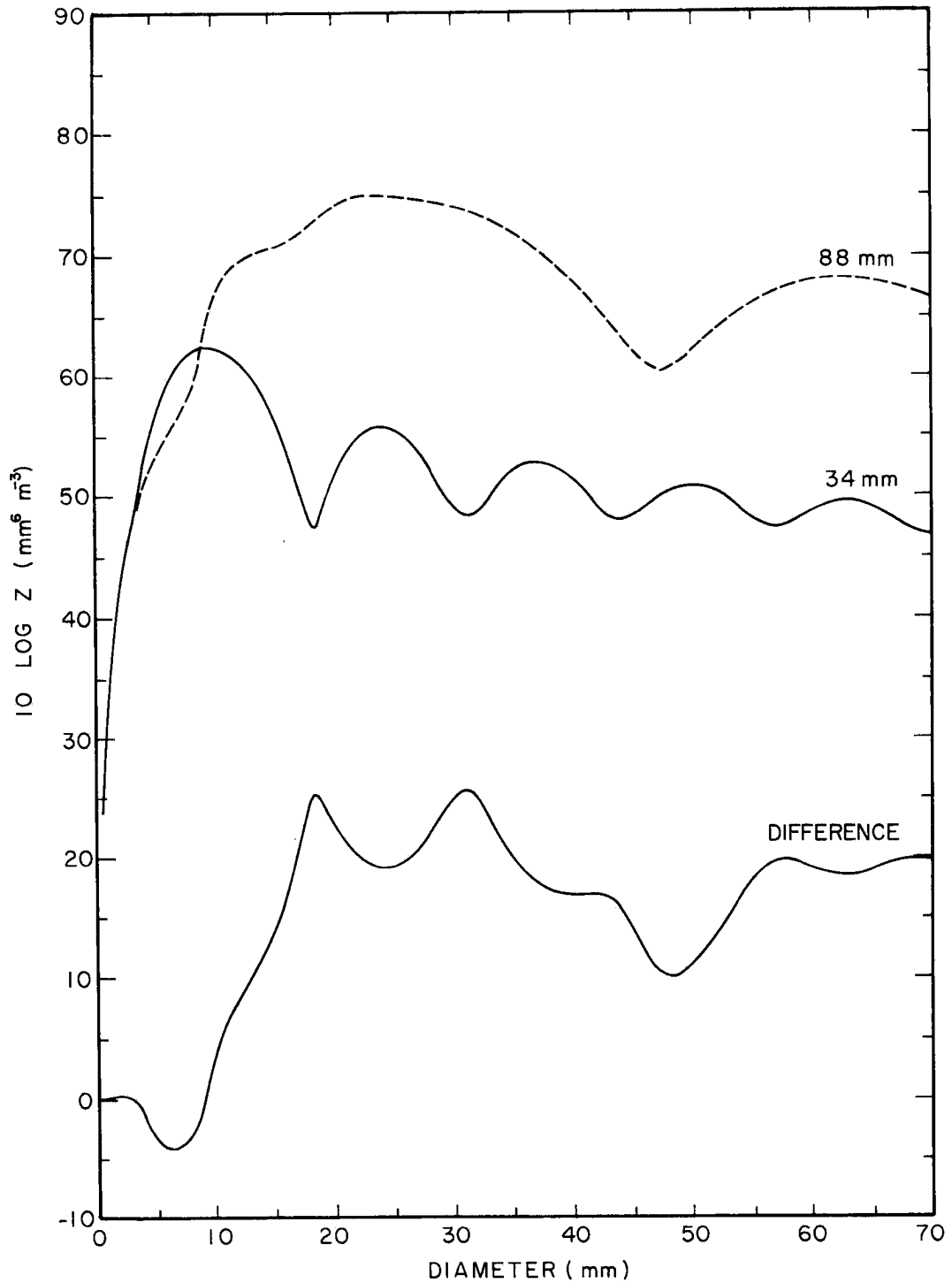


Figure 2.2. Reflectivity of wet hail as a function of diameter for 88 and 34 mm radar waves and, at the bottom, the difference between them in dB. (1 g m^{-3} , 0°C , Z in $\text{mm}^6 \text{ m}^{-3}$)

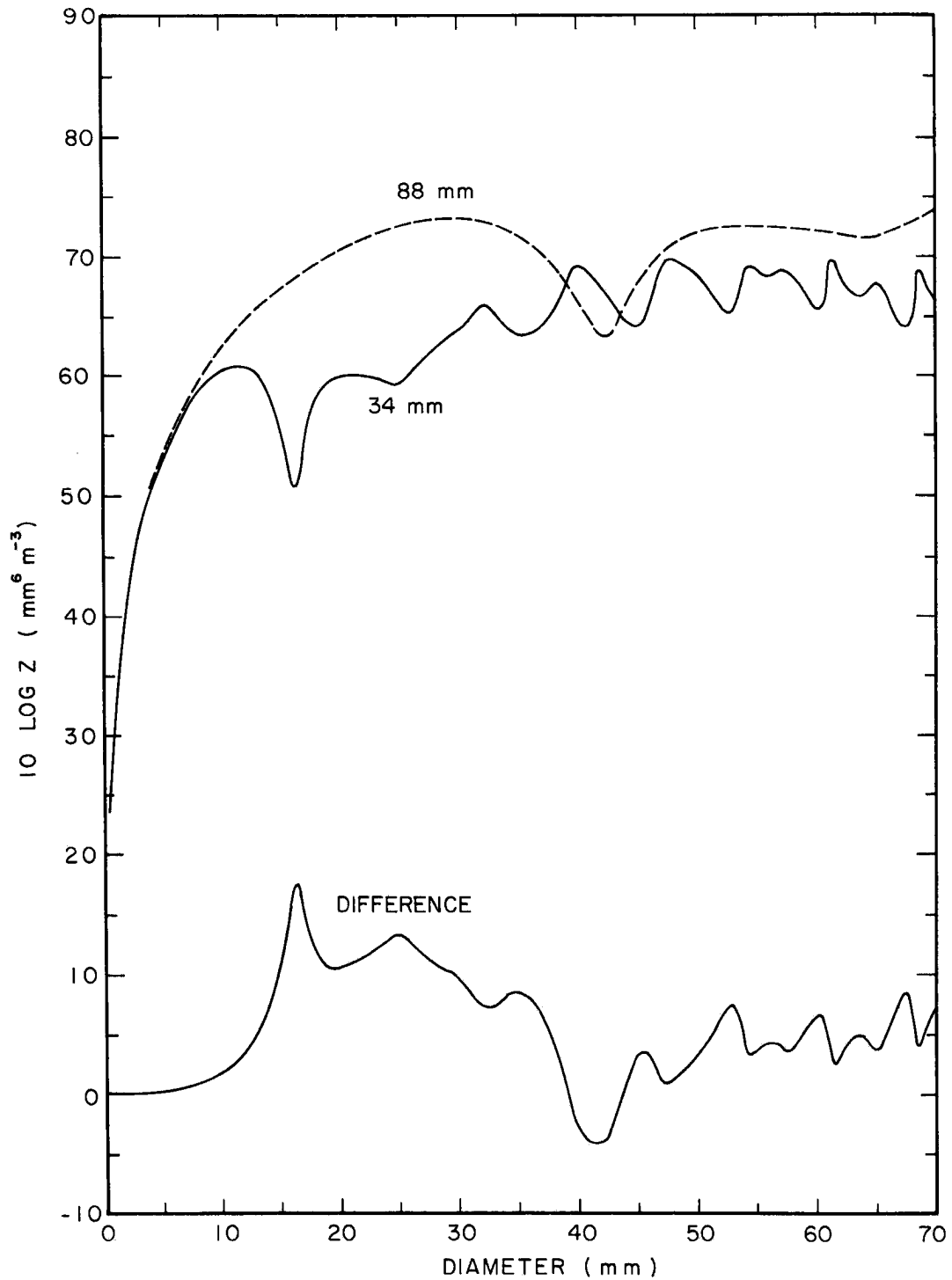


Figure 2.3. Reflectivity of dry hail as a function of diameter for 88 and 34 mm radar waves and, at the bottom, the difference between them in dB. (1 g m^{-3} , 0°C , Z in $\text{mm}^6 \text{ m}^{-3}$)

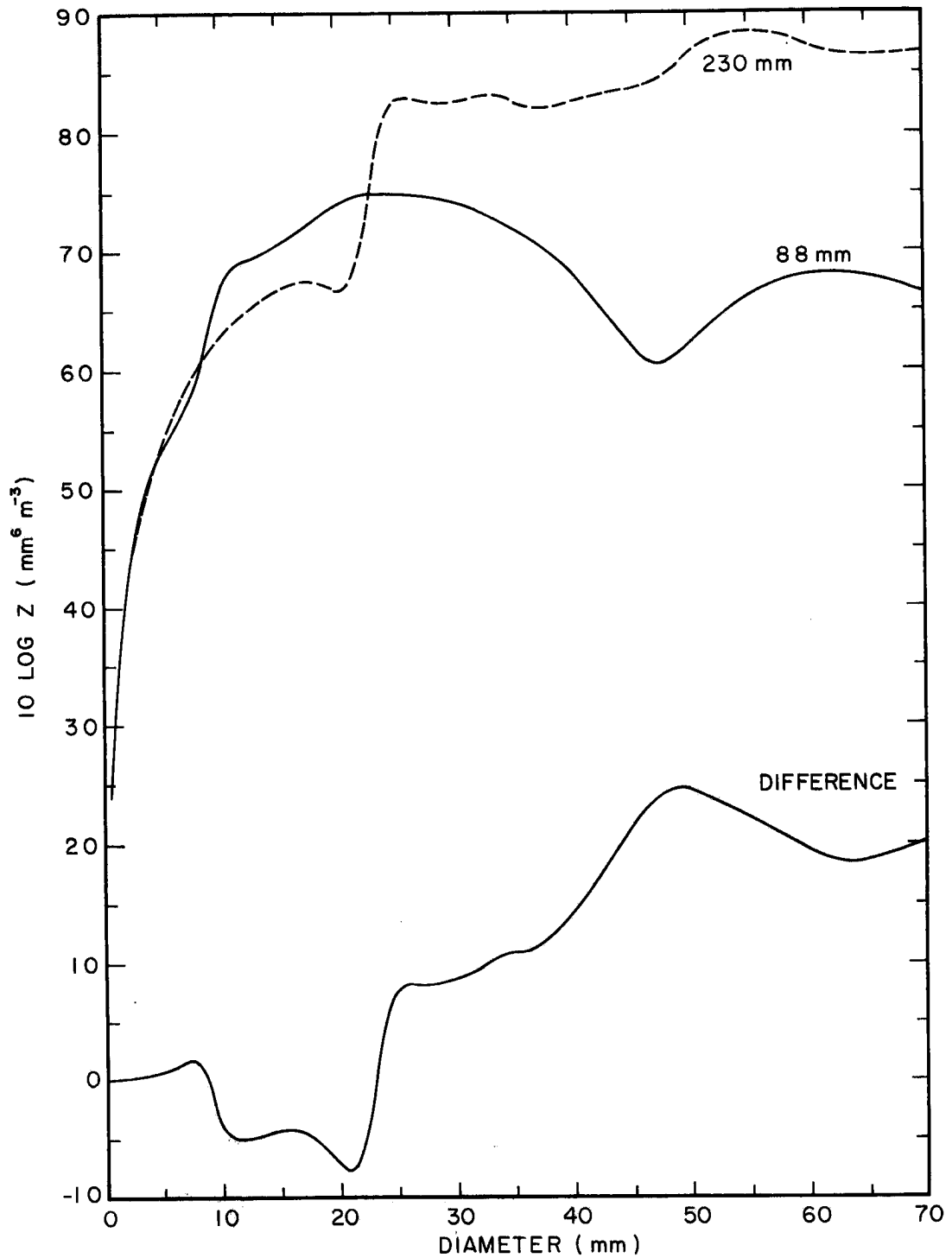


Figure 2.4. Reflectivity of wet hail as a function of diameter for 230 and 88 mm radar waves and, at the bottom, the difference between them in dB. (1 g m^{-3} , 0°C , Z in $\text{mm}^6 \text{ m}^{-3}$)

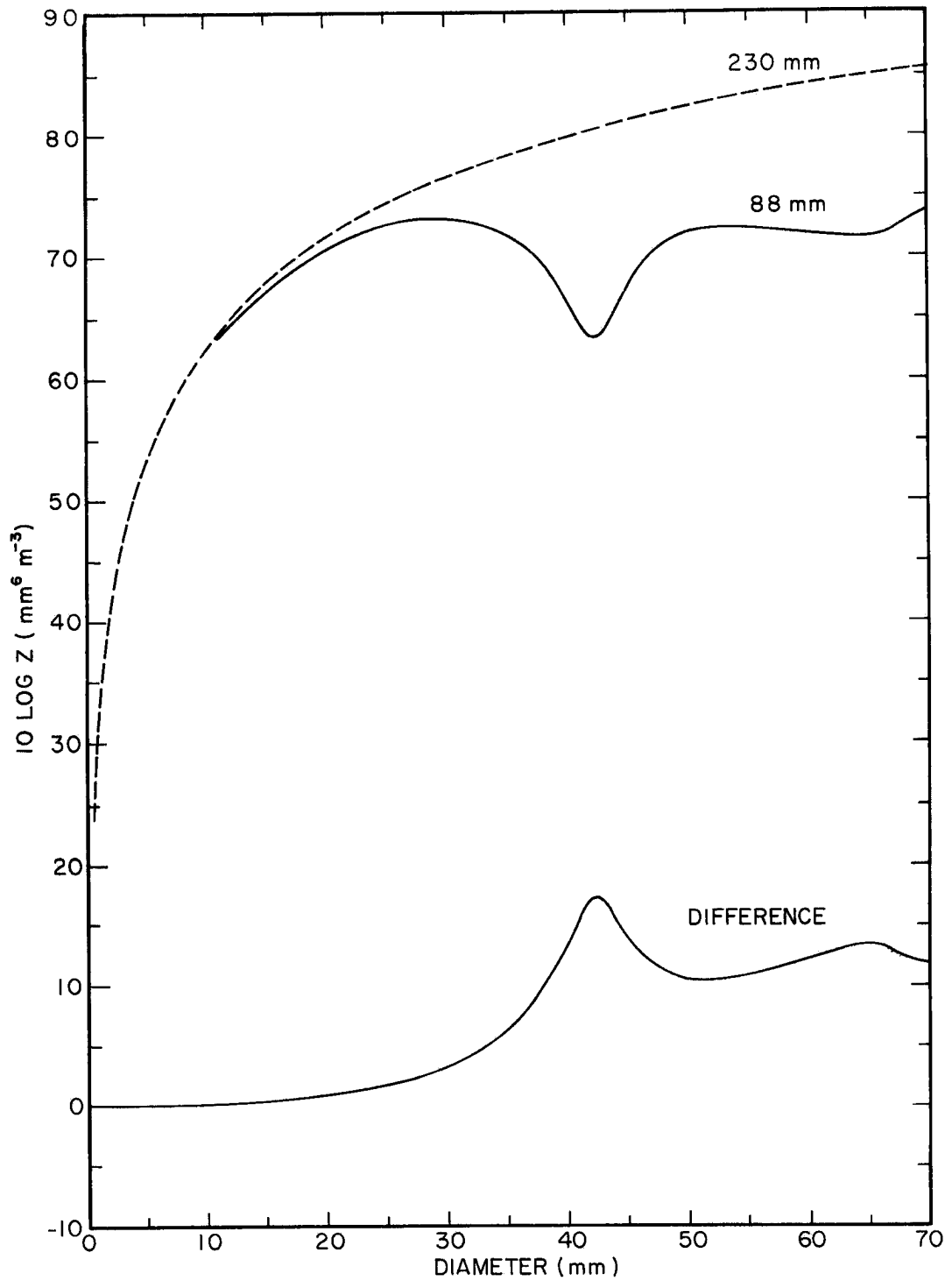


Figure 2.5. Reflectivity of dry hail as a function of diameter for 230 and 88 mm radar waves and, at the bottom, the difference between them in dB. (1 g m^{-3} , 0°C , Z in $\text{mm}^6 \text{ m}^{-3}$)

Even with a 2 dB error in reflectivity measurement at either wavelength, such hail growth could easily be noticed by continuously monitoring the reflectivities of the suspected growth zone. Before any hail growth begins, the reflectivity will be the same at both wavelengths, and the observed difference will be zero. As the hailstones form and grow to about 7 mm in diameter, the 34 mm reflectivity initially increases at a more rapid rate than the 88 mm reflectivity, resulting in a negative difference. As the hailstones continue to grow, to approximately 18 mm diameter, the 88 mm reflectivity continues to increase while the 34 mm reflectivity reaches its absolute maximum at 9.8 mm diameter and then rapidly decreases to a relative minimum at 18.3 mm diameter. This causes the reflectivity difference to increase from -4.1 dB at 6.7 mm diameter to 25.4 dB at 18.4 mm diameter.

As the particles reach large sizes it is not possible to determine the particle size exactly. For example, a difference of 21 dB could correspond to diameters of 17.0, 21.1, 27.3, or 34.2 mm assuming no error in the measurements. When a 2 dB error is considered, the particles could be any size from 16.5 to 35.7 mm, 55.9 to 70.8 mm, or 94.1 to 97.2 mm. But it can be concluded that a difference of 20 dB implies the presence of at least moderate-sized hail.

Figure 2.3 shows the results for 1 g m^{-3} of ice spheres at wavelengths of 88 and 34 mm. Dry hail probably reflects like ice spheres, and it is most likely to be found in regions near the top of the cloud where the temperature is colder than -20°C . The scattering function for ice at 34 mm wavelength has numerous maxima and minima, making it virtually impossible to measure the size of dry hail with 88 and 34 mm wavelength radars. If one observes a difference of 5 dB and assumes a 2 dB uncertainty in the accuracy of the reflectivities, the hail could be in any one of a large number of size ranges.

The reflectivity of wet hailstones at 230 and 88 mm wavelengths is shown in Figure 2.4. These calculations were performed to investigate the usefulness of two long wavelengths in detecting monodisperse wet hail. Growth of hail from embryo size to approximately 7 mm diameter would not be noticed because the difference is small and changes only slightly. Growth from 8 to 21 mm diameter could be

observed, but not with great precision. For a -5 dB difference, one could confidently state that the hailstones were between 10 and 20 mm diameter (grape size). Growth from 21 to 25 mm diameter is easily noticeable; note how the difference increases rapidly in this interval. The difference increases fairly uniformly and rapidly from 25 to 50 mm diameter, and growth should be observable by monitoring the reflectivity difference. At diameters over 50 mm it would not be possible to estimate the hail size since more than one size corresponds to most values of the difference. It is obvious, however, that a 20 dB difference, observed with 230 and 88 mm radars, would indicate the presence of large hail (golf-ball size or larger) in the cloud.

Figure 2.5 presents the results for dry hail observed at 230 and 88 mm wavelengths. Growth of hail from 0 to 30 mm diameter is not observable because the difference is small and it increases very slowly with particle diameter. Growth from 30 to 42 mm diameter may be observable. Measurement of larger hail sizes is not feasible because the difference function becomes oscillatory, and more than one size corresponds to most values of the difference.

One advantage of using 230 and 88 mm radars in studying hailstorms is that both wavelengths are unattenuated, making dual-wavelength measurements in the core of the storm possible. Useful measurements in the accumulation zone, where the hail is probably wet, might be made with two long wavelengths. A disadvantage of the 230 mm set is that a large antenna is required to obtain a 1° "pencil-beam" which is required for good resolution.

Reflectivity of exponential hail size spectra

Since it appears to be physically unrealistic to assume that the hailstones will be of uniform size, an analysis which considers a spectrum of hailstone sizes would seem more appropriate. In an area of strong updrafts it may be possible that the updraft supports a relatively small number of large particles in a zone near the updraft maximum. The Soviet scientists (Sulakvelidze *et al.*, 1965) have termed this area an "accumulation zone." This is the zone where hail growth is believed to take place. Larger particles suspended in the updraft probably grow by accretion of smaller supercooled water

droplets being carried up through this zone by the updrafts. One would thus encounter a spectrum of hail sizes, with a few large particles and numerous smaller ones. Analysis of ground hail samples by Douglas (1964) indicated that the stones were exponentially distributed according to their size. It has been shown by Marshall and Palmer (1948) and by Gunn and Marshall (1958) that raindrops and aggregate snowflakes may also follow exponential distributions.

One could therefore consider an exponential distribution of the form

$$N_D = \int_D^{D + \Delta D} N_0 e^{-\Lambda D} dD \quad (2.73)$$

as a first approximation to the spectrum of hail sizes present in an accumulation zone. Here, N_D denotes the number of particles with diameters between D and $D + \Delta D$. N_0 is a constant directly proportional to the number concentration and it is given the value of $4 \text{ m}^{-3} \text{ mm}^{-1}$, which was used by Atlas and Ludlam (1961). The parameter Λ , with the units of mm^{-1} , is related to the rapidity at which the number concentration of particles decreases as the particle diameter increases. It is also related to the mass density of the entire spectrum. For $\Lambda = 0$, there is an equal number of particles in each 1-mm size interval. If Λ is positive, the number of particles in a specified size interval drops off exponentially according to the particle diameter. Naturally, the larger the value of Λ , the faster the rate at which the particle concentration drops off with size. Large positive values of Λ result in low spectral mass densities while small positive values of Λ gives high spectral mass densities.

Calculations were performed in order to determine the effect of maximum particle diameter in the spectrum upon the difference between the 88 and 34 mm reflectivities. In these calculations, the lower limit of each spectrum was held at 1 mm diameter while the upper limit was varied in 1 mm steps from 1 mm to 80 mm diameter. The integrations were carried out in 1-mm increments. Computations were done for spectra with values of Λ of .13, .15, .18, .21, .25, and .30 and corresponding mass densities of 41.9, 24.3, 11.9, 6.5, 3.2, and 1.6

g m^{-3} respectively. The mass densities were computed assuming lower and upper limits of 0 and 60 mm diameter, respectively and using 1-mm integration steps. The densities of water and ice were assumed to be 1.0.

Figure 2.6 shows the reflectivity difference as a function of maximum particle diameter in exponential spectra of wet hailstones. Four spectra are shown, having values of Λ of .13, .18, .25, and .30. When all the particles in a spectrum are small, the reflectivity difference is nearly zero. As larger particles are added to the spectrum in accordance with (2.73), the reflectivity difference first becomes negative. This occurs because particles between 3.1 and 8.9 mm diameter reflect stronger at 34 mm than at 88 mm. The largest negative difference occurs at 7 mm diameter. When still larger particles are added, the difference becomes positive and increases to a terminal value which depends on the value of Λ . A small value of Λ results in a relatively large terminal value of the difference while a large value of Λ yields a smaller difference. This is physically reasonable since it has already been shown in Figure 2.2 that large particles reflect more at 88 mm than at 34 mm, and with smaller values of Λ one would have larger concentrations of large particles. Figure 2.6 implies that growth of hailstones from diameters of 7 mm to about 20 mm can be observed by continuously monitoring the reflectivities observed at 88 and 34 mm wavelengths. However, it is not possible to measure particle diameters exceeding 20 mm because the reflectivity difference curves level off.

Figure 2.7 is similar to Figure 2.6 except that dry hail rather than wet hail is being considered. As in Figure 2.6, the reflectivity difference is initially zero when all the particles are small. When larger particles are added to a spectrum, the reflectivity difference increases to an absolute maximum, drops off somewhat, and then levels off to a terminal value which depends on Λ . But here, a small value of Λ does not necessarily imply a larger terminal value of the difference than a large value of Λ . This can be explained by referring to Figure 2.3. When one considers ice spheres, it can be seen in Figure 2.3 that the large particles don't necessarily have the largest reflectivity differences. In fact, the difference function for large

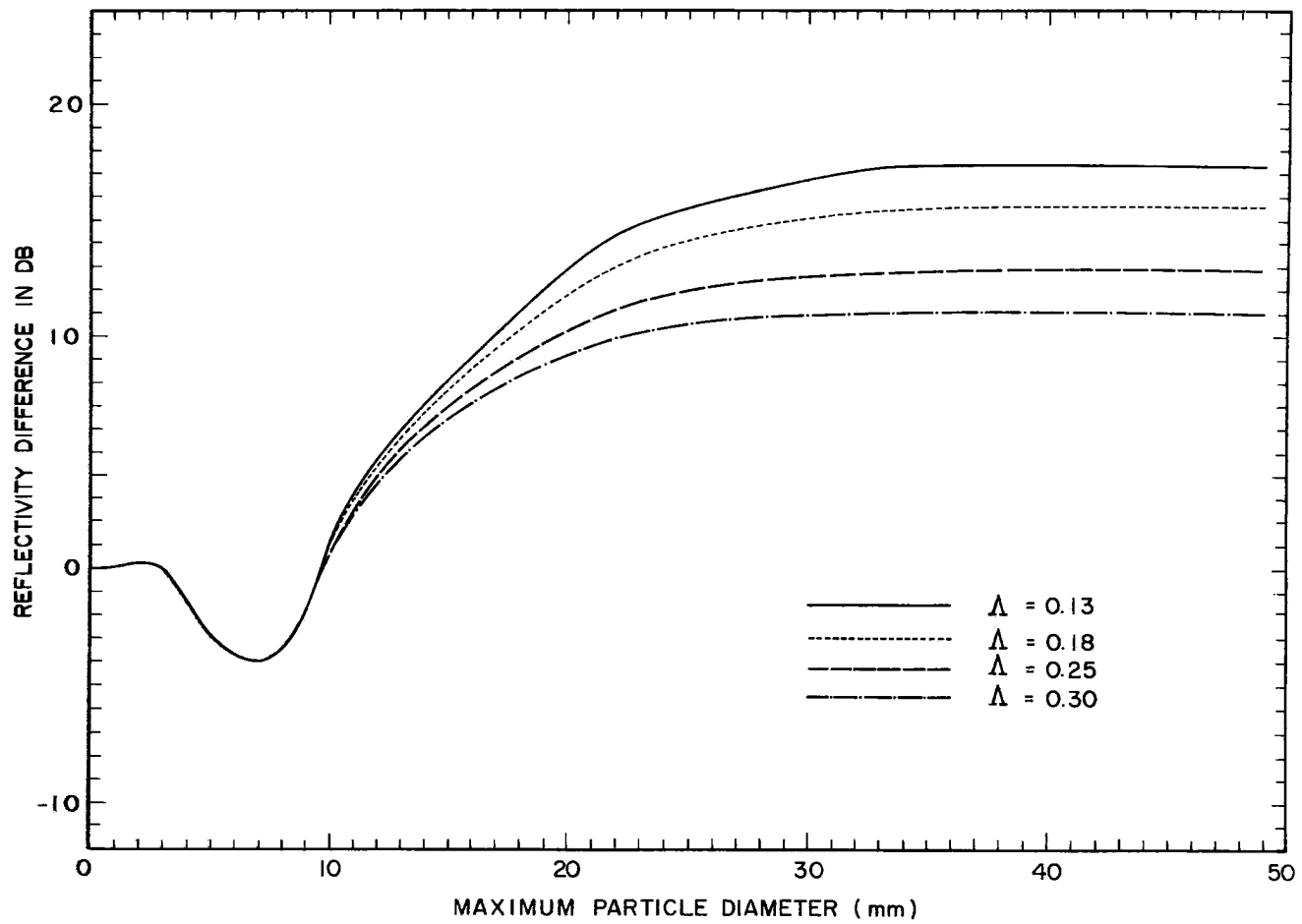


Figure 2.6. The difference between the reflectivities at 88 and 34 mm as a function of maximum particle diameter contained in exponential spectra of wet hailstones.

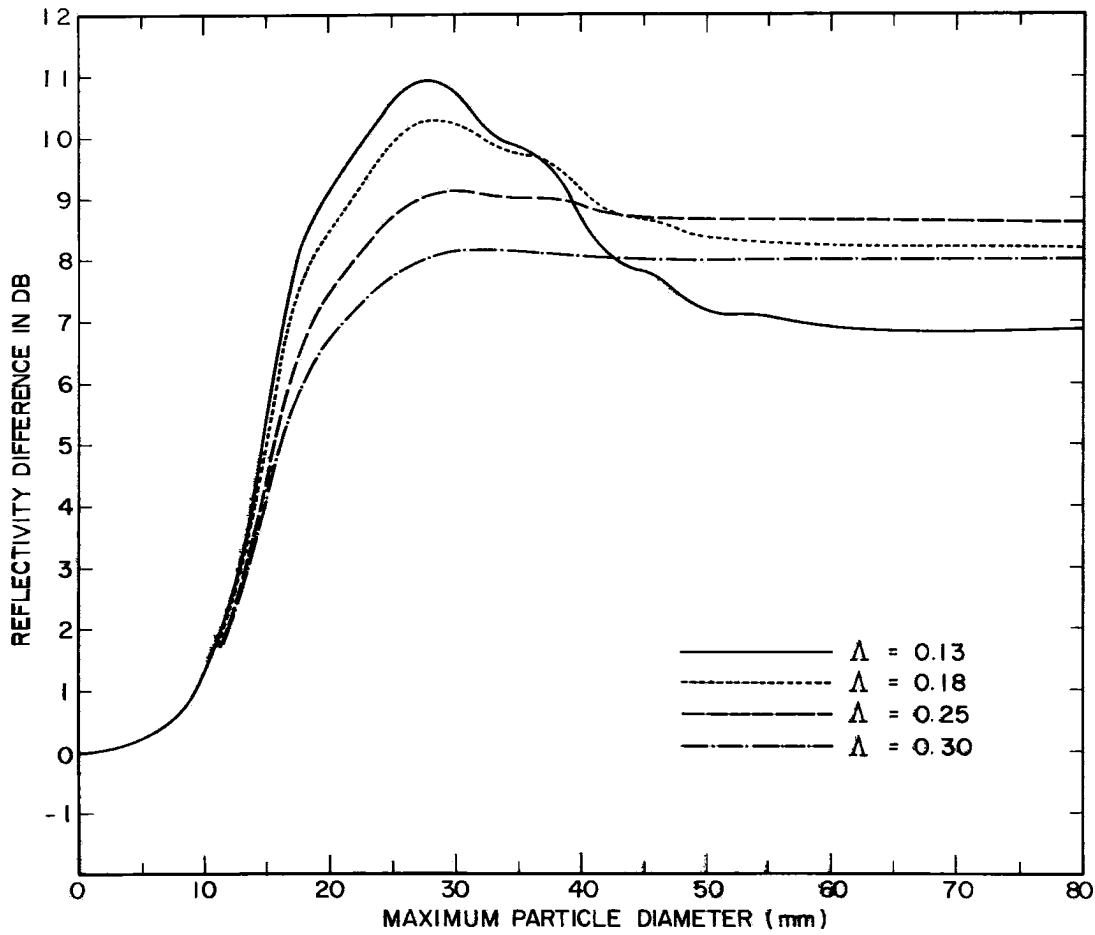


Figure 2.7. The difference between the reflectivities at 88 and 34 mm as a function of maximum particle diameter contained in exponential spectra of dry hailstones.

particles is usually less than that for the intermediate-size particles. Since the median particle diameter is not the same in all spectra shown, one could expect, in a very general way, the results shown.

The reflectivity difference increases from 0 dB when there is no hail to 8-11 dB when there is 25 mm hail present. One should be able to detect an increase in hail size from about 5 to 25 mm by observing the 88 and 34 mm reflectivities. Because the difference varies less than in the case of an exponential spectrum of wet hailstones, greater accuracy in measurement of reflectivity would be required. An error of 2 dB would probably be the maximum that could be tolerated. Such accuracy should be obtainable with well-calibrated radars. As in the case of wet hail, it is not possible to measure large hail diameters because the difference curves level off at large sizes.

Chapter III
RADAR EQUIPMENT AND DATA REDUCTION PROCEDURES

Description of the Radar Equipment

The radars used in the 1968 hailstorm studies are those in a modified M33. The M33 radar system consists of an acquisition radar operating at 88 mm wavelength and a track radar operating at 34 mm. The 34 mm radar was operated with its tracking scanner on giving an effective beamwidth for resolution of 30 milliradians. The characteristics of these radars are presented in Table 3.1.

Table 3.1. M33 Radar Characteristics

	<u>Acquisition</u>	<u>Track</u>
Peak transmitted power	600 kw	200 kw
Beamwidth (milliradians)	30 (circular)	20 (circular)
Wavelength	88 mm	34 mm
Minimum detectable signal	-105 dBm	-105 dBm
Pulse length (microsec.)	1.35	0.25
Antenna dimensions	Parabolic dish 3.66 m diameter	Waveguide lens 2.06 m diameter
Antenna gain	35.5 dB	38 dB
Pulse repetition rate	833 sec ⁻¹	833 sec ⁻¹
Polarization	Vertical	Vertical
Types of echo presentation	PPI, RHI, A	A

Reflectivity measurements at 88 mm

Real-time records of reflectivity are made by attenuating the signals in a linear IF amplifier down to a calibrated reference level on an A-scope. Records are also made by photographing either a PPI or an RHI scan fed from a logarithmic IF amplifier. Calibration signals are also photographed. Reflectivity data are obtained by scanning the negatives with a microdensitometer. A slow scan speed, 8 deg sec⁻¹, is used on PPI and RHI scans to give good averaging of the received signals.

Reflectivity measurements at 34 mm

Storm reflectivity is recorded by using the AGC voltage which results from signals in the range gate. Signals are recorded on chart paper as the antenna moves slowly in elevation with the range gate fixed at the location found to have the strongest signal. Calibration signals are also recorded.

Radar calibration procedure

Both radar receivers were calibrated with signal generators connected into the waveguides through directional couplers. These calibrations were done at the end of each day's operations. In addition, during long periods when there were numerous echoes under surveillance, the 88 mm radar was calibrated at hourly intervals to check for drift in the calibration. The gain of both antennas was measured using a 253 mm diameter sphere suspended from a sounding balloon.

Calculation of observed reflectivity values

Values of received power are extracted from the photographic and strip-chart records from the 88 and 34 mm radars. Reflectivity is computed using a modified form of the Probert-Jones meteorological radar equation (Bushnell, 1967):

$$Z = \frac{22.89\lambda^2 R_o^2 P_r}{hL^2 G^2 \theta_1 \phi_1 |K|^2 P_t} \quad (3.1)$$

Here, h is the pulse length in meters, L the losses in the directional coupler and cable in dB, G the antenna gain in dB, θ_1 and ϕ_1 the vertical and horizontal half-power beamwidths, R_o the range in m, P_r the received power in dBm, and P_t the peak transmitted power in dBm.

Chapter IV
TOPOGRAPHY AND CLIMATOLOGY
OF NORTHEASTERN COLORADO

The radars are located on a small rise about 3 km north-northeast of New Raymer, Colorado. The elevation of the radar site is about 1,480 m, and the horizon is unobstructed in all quadrants. There are relatively few sources of ground return. Figure 4.1 shows a map of the region in northeastern Colorado where the 1968 hailstorm studies were conducted. This area consists of a broad, high plain with the Front Range of the Rocky Mountains lying about 150 km west of the radars. The plain is cut by the South Platte River which runs from west-southwest to east-northeast. Elevations vary from about 1,100 m in the lower portions of the South Platte River Valley to about 1,900 m near Cheyenne, Wyoming. The terrain north of New Raymer is characterized by numerous hills, buttes, gullies, and intermittent creek beds. Convective activity frequently begins over this higher region earlier in the day than over the remainder of the area.

For most stations in the area, May is the wettest month. Precipitation amounts in May exceed 80 mm along the eastern foothills of the Rocky Mountains and along Colorado's eastern border. The precipitation amounts generally decrease in succeeding months, and by September, few stations receive over 35 mm. Most of the precipitation is associated with frontal convective activity. During July and August, mean daily maximum temperatures reach 30°C and daily maxima of 35°C or higher are not uncommon. On most thunderstorm days the dew point reaches or exceeds 10°C. Hailstorms over the high plains occur most frequently during the month of June (Visher, 1954). Northeastern Colorado and southeastern Wyoming have the highest frequency of hailstorms in the United States. Weather Bureau climatological records show that, on the average, a station in this area experiences more than 7 hail days per year. (Visher, 1954)

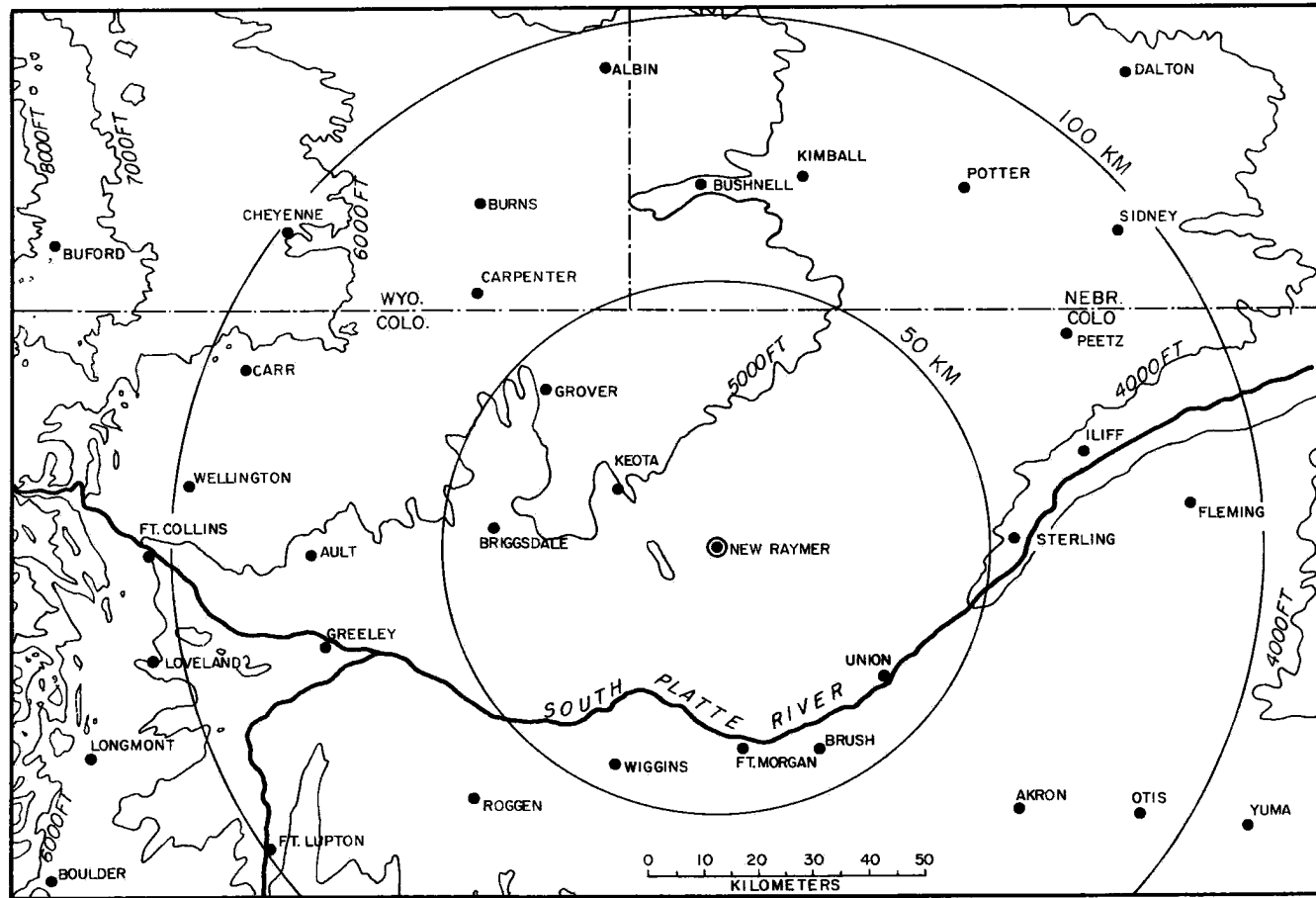


Figure 4.1. Map of the region in northeastern Colorado used in the 1968 hailstorm studies.

Chapter V

DUAL-WAVELENGTH RADAR OBSERVATIONS OF A SEVERE HAILSTORM OVER NORTHEASTERN COLORADO

Radar observations of hailstorms were made during the entire summer of 1968 and records were made on several good storms. The storm that seems most suitable for study occurred at sunset on 28 July 1968 about 70 km east of the radar sets.

The synoptic situation

The storm was one of only two which occurred within 100 km of the radars on this date. Scattered thunderstorms were also being reported by stations in Wyoming, western Kansas and Nebraska, and southeastern Colorado. The surface wind flow was dominated by a large high pressure system centered over the Canadian Prairie Provinces. The surface winds over northeastern Colorado at the time of the storm were generally light and variable, but having an easterly component. The surface dew points reached 17°C along Colorado's eastern border at 1700 MDT. There were no significant fronts near the area. Figure 5.1 shows the surface chart at 0500 MDT on 28 July 1968.

The upper winds were from the northwest at altitudes above 6 km MSL. The wind speed was generally light with the greatest speed being 18 m sec^{-1} at 12 km. The dynamical effects of vertical wind shear on storm development (Modahl, 1969) were not significant. A ridge and a closed high at 500 mb were located over the Rocky Mountain states. Figure 5.2 shows the 500 mb chart for 0500 MDT on 28 July 1968.

Soundings taken from Fort Collins at 1100 MDT and Denver at 1700 MDT indicated that the atmosphere was relatively dry at intermediate and high levels. There was a thin moisture layer near the surface. The 1700 MDT sounding showed a steep temperature lapse rate, $10.8^\circ\text{C km}^{-1}$, from the surface to 600 mb. The height of the cloud base was computed to be 2.9 km, assuming a 14% surface moisture deficit (Renné, 1969).

Case history of the storm

The storm was first observed on radar about 20 km north of Sidney, Nebraska, at about 1900 MDT. Locally high winds from a small,

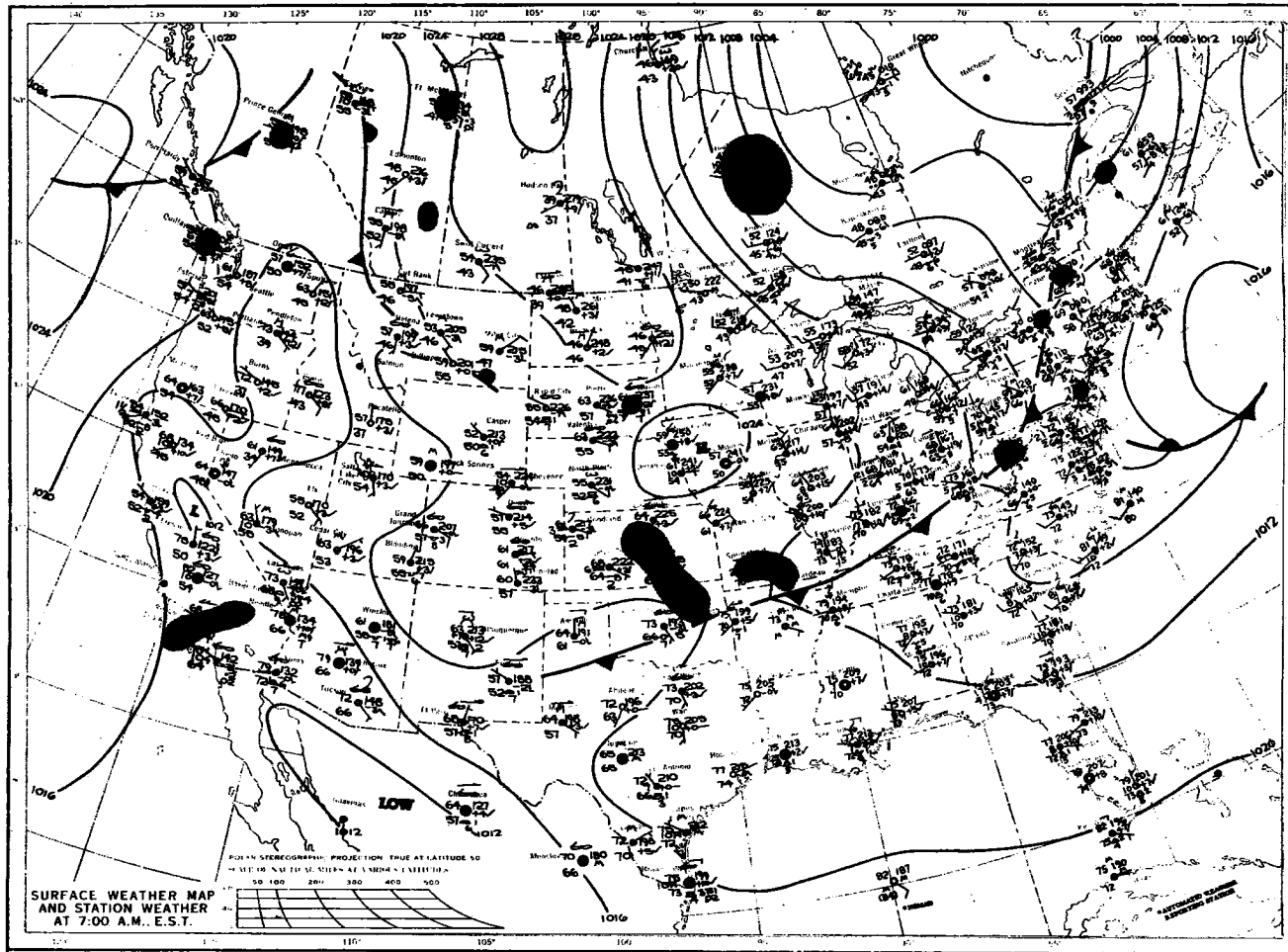


Figure 5.1. Surface chart for 0500 MDT on 28 July 1968.

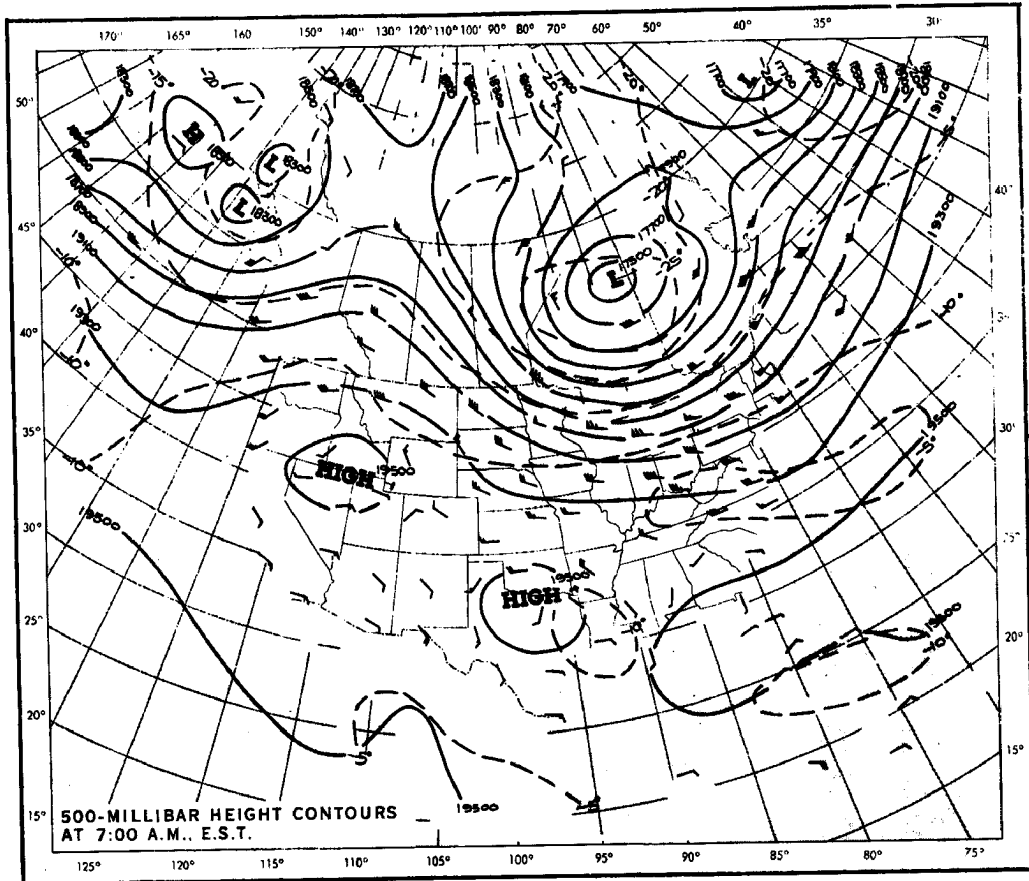


Figure 5.2. 500 mb chart for 0500 MDT on 28 July 1968.

dissipating cumulonimbus over the radar site made it difficult to rotate the radar antennas, and data collection did not begin until 1931 MDT. The following day a field survey of the storm was made in which the local residents were asked about the size and amount of hail. Figure 5.3 shows positions of hail reports with respect to the location of the radars. The times of the individual reports are not shown as they were not considered reliable. Hail from this storm was also reported in regions north of the area shown. The reports show that the storm dropped hailstones of up to golf-ball size from a point about 20 km north of Sidney, Nebraska, to a point about 25 km northeast of Akron, Colorado. The width of the hail track varied from 4 to 6 km. The maximum 88 mm reflectivities measured at low elevation angles, taken from continuous PPI photographs, are shown in Figure 5.4. There were three periods of high storm intensity when the value of $10 \log Z$ exceeded 70. Figure 5.5 shows PPI photographs of the storm taken at approximately 10-minute intervals. Radar and visual cloud top heights were measured routinely using the 34 mm radar (Figure 5.6). In general the tops were highest during the most intense phases of the storm.

There was a strong correlation between high 88 mm reflectivity and presence of large hail on the ground. The field survey showed three locations of intense hailfall with stones of grape size or larger. The hail reached golf-ball size in two of the areas. In the third area there were large amounts of grape-sized hailstones. The storm had high reflectivity near these positions at 1945, 2031, and 2105 MDT. The largest distance between the location of hailfall on the ground and the location of high storm reflectivity was at 2105 when the storm was 3 km south of the hail found on the ground. At 2016 there was a high 88 mm reflectivity. Grape-sized hail was found at this position where the storm was getting stronger as it passed over higher ground south of the South Platte River. The maximum observed 34 mm reflectivity (Figure 5.7) was only weakly related to either high values of the 88 mm reflectivity or large hail observed on the ground. It should be noted, however, that the usefulness of this radar in the study of severe storms is severely limited by attenuation.

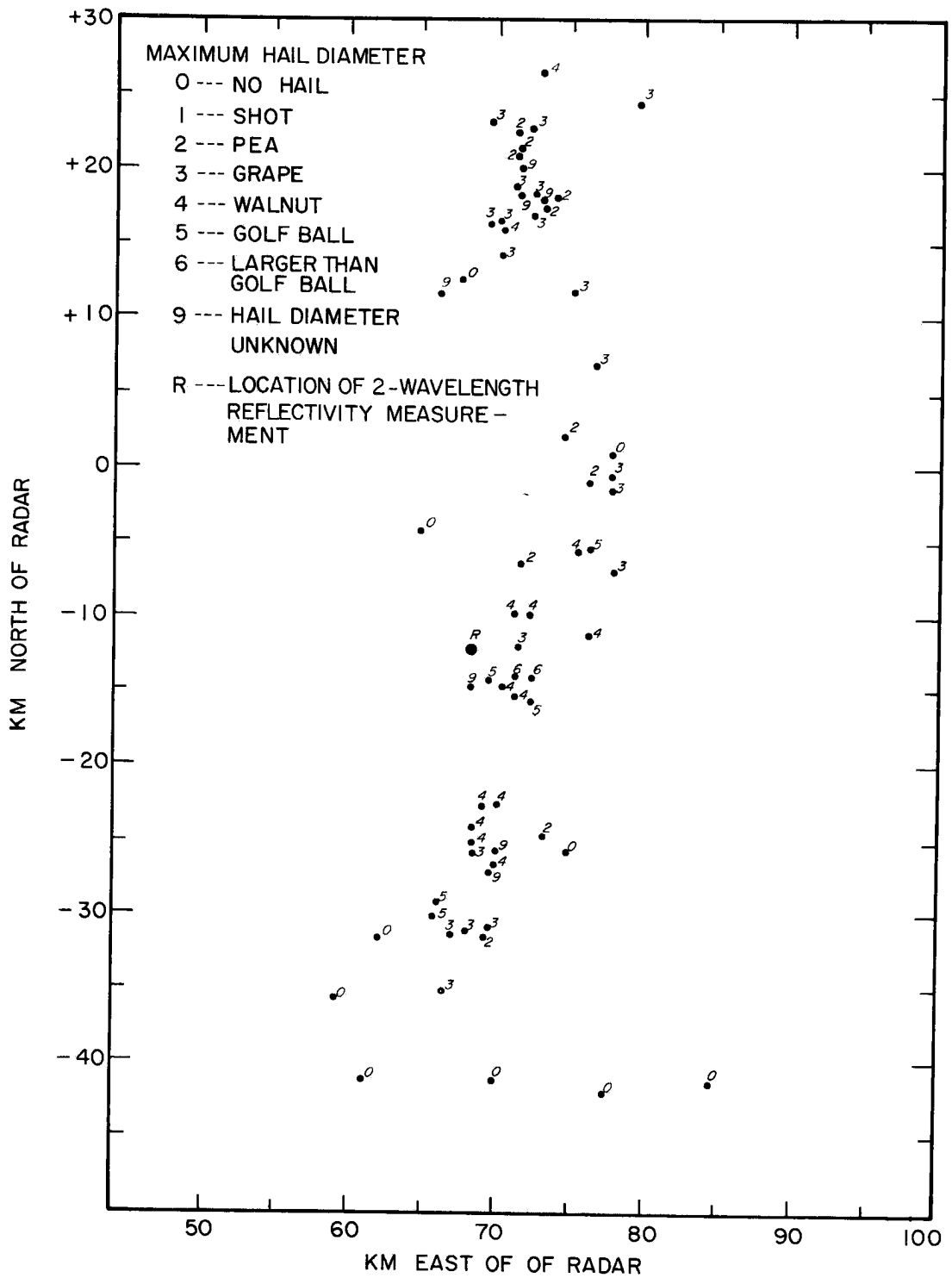


Figure 5.3. Hailfall from the storm of 28 July 1968.

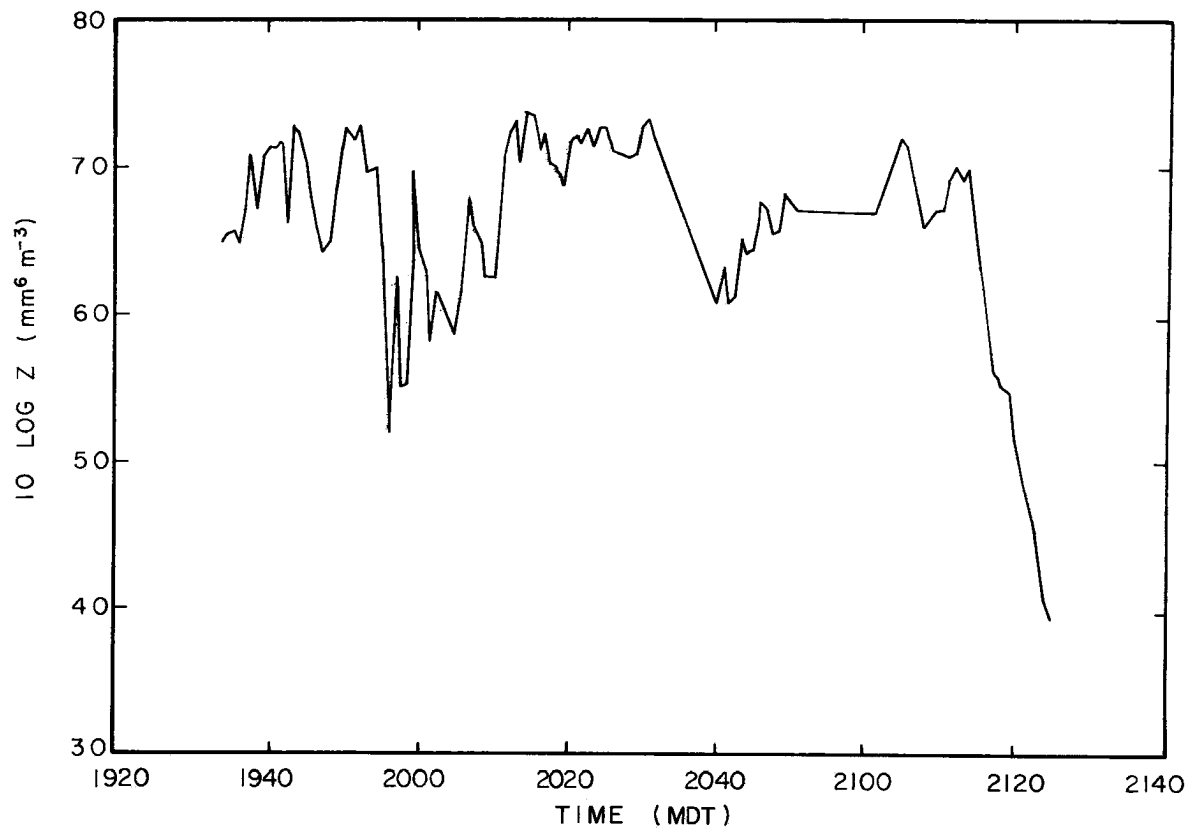


Figure 5.4. Maximum 88 mm reflectivity of the hailstorm of 28 July 1968, measured at low elevation angles.

Time (MDT)	Elevation Angle
1934-1956	2.8°
1957-1959	4.2°
2000-2032	2.4°
2040	5.4°
2041	4.2°
2042-2126	3.2°

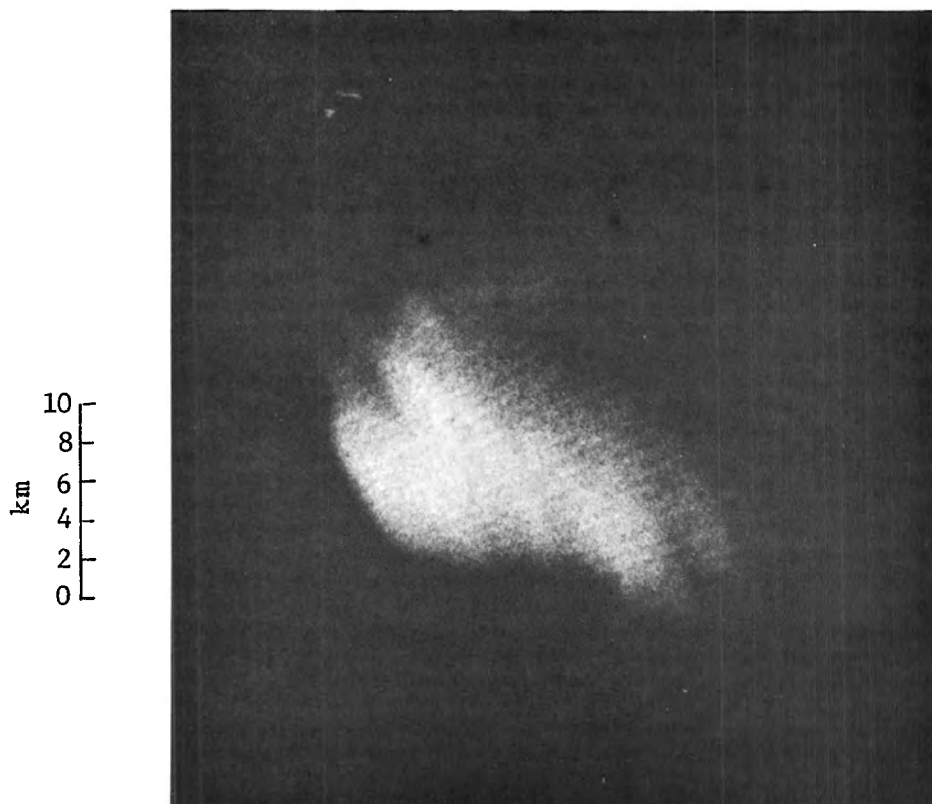


Figure 5.5a.
19:35:00 MDT
Elevation Angle 2.8°
 $10 \log Z_{\max} = 65.4$

Figure 5.5. 88 mm PPI photographs of the storm of 28 July 1968. North is to the top. Scale: 1 cm = 4 km.

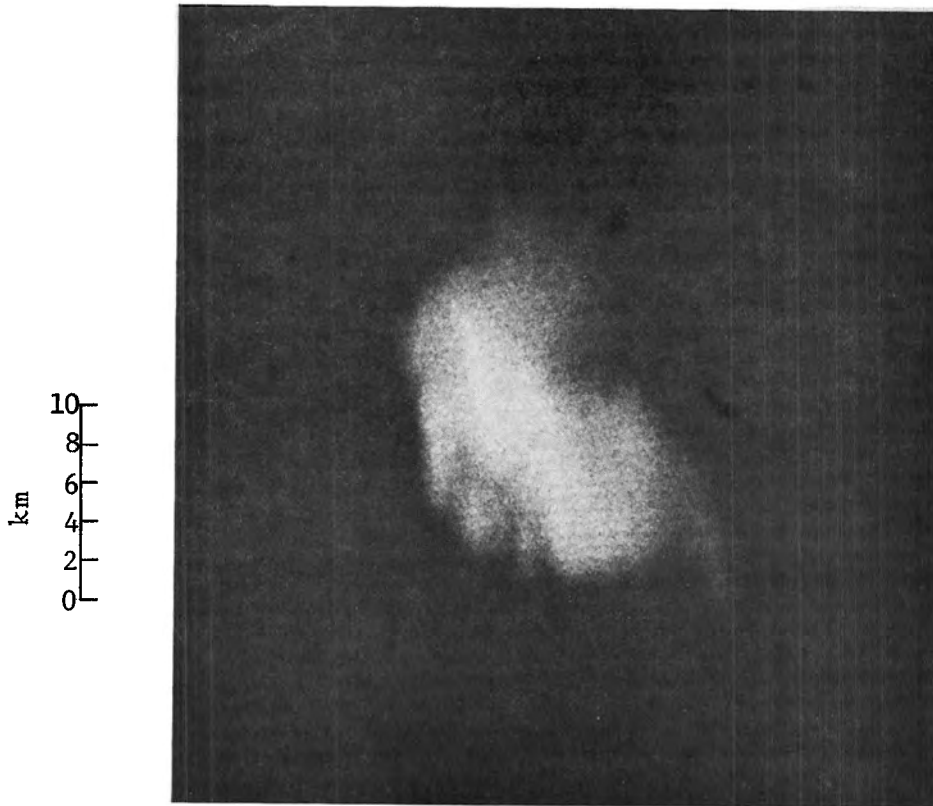


Figure 5.5b.
19:44:50 MDT
Elevation Angle 2.8°
 $10 \text{ Log } Z_{\text{max}} = 72.3$

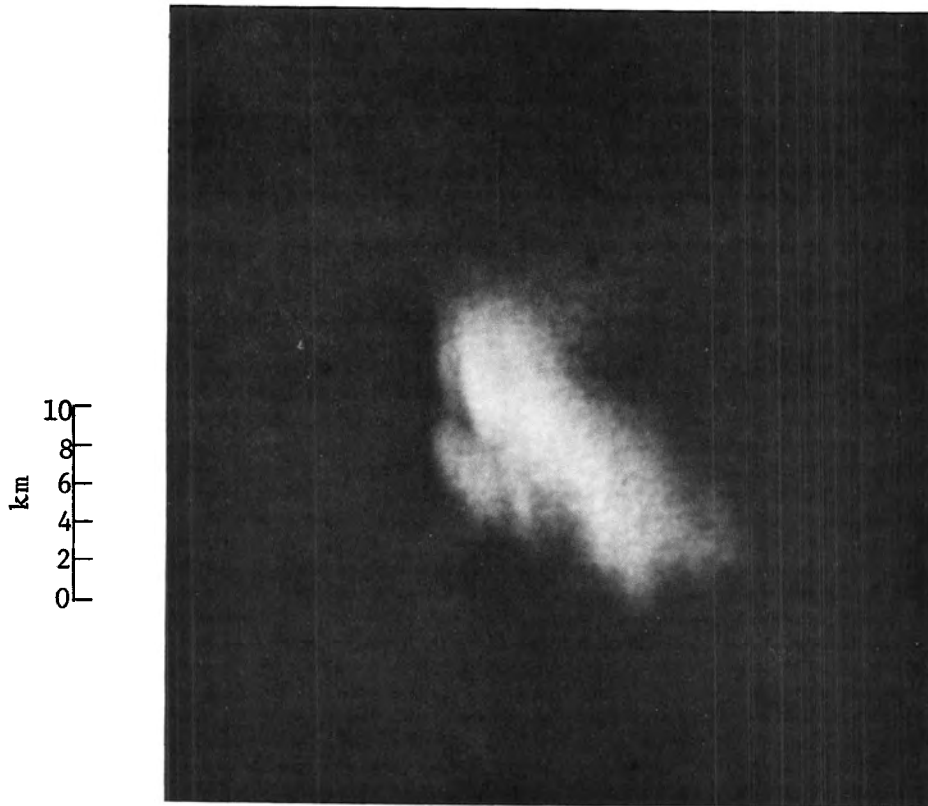


Figure 5.5c.
19:55:20 MDT
Elevation Angle 2.8°
 $10 \text{ Log } Z_{\text{max}} = 69.9$

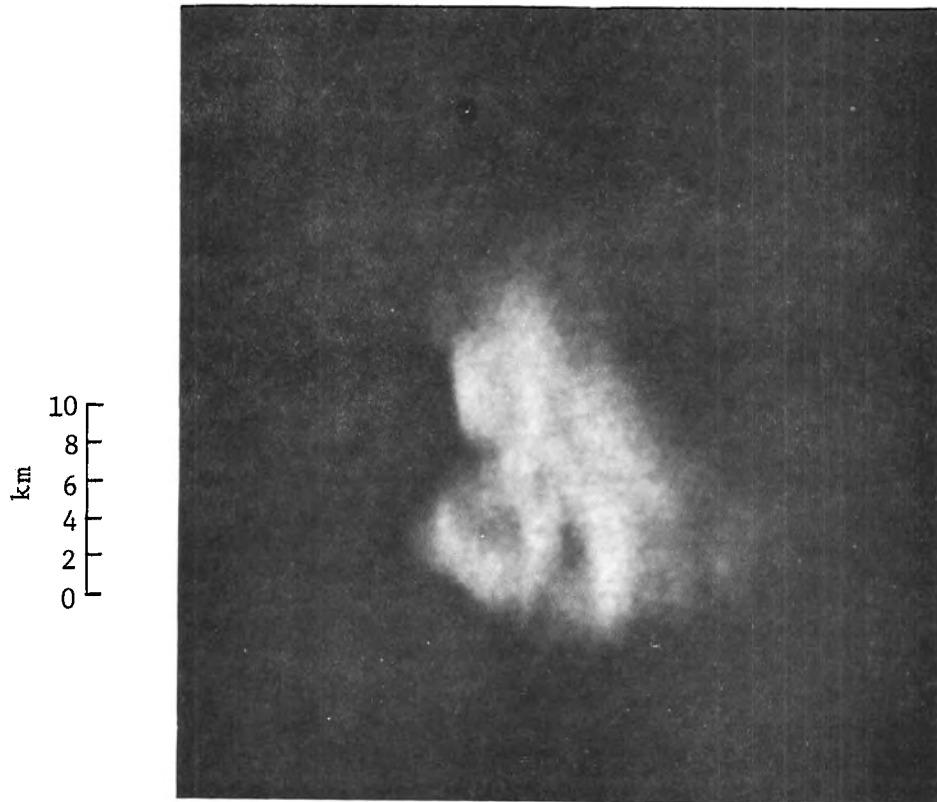


Figure 5.5d.
20:05:00 MDT
Elevation Angle 2.4°
 $10 \text{ Log } Z_{\text{max}} = 59.5$



Figure 5.5e.
20:15:20 MDT
Elevation Angle 2.4°
 $10 \text{ Log } Z_{\text{max}} = 73.7$

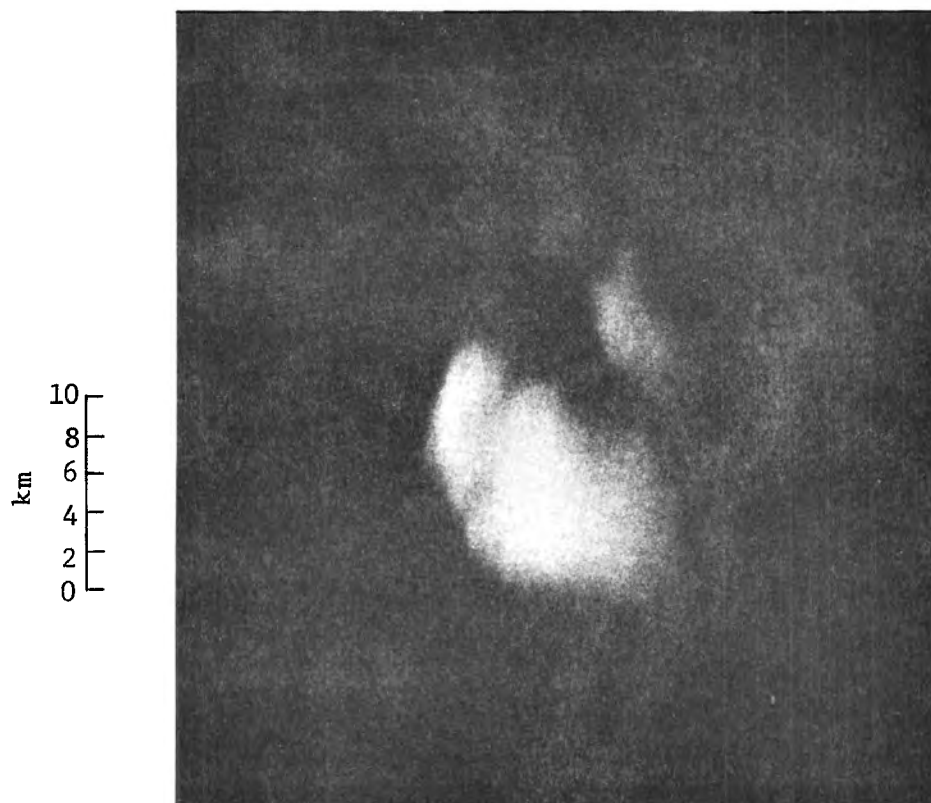


Figure 5.5f.
20:25:00 MDT
Elevation Angle 2.4°
 $10 \text{ Log } Z_{\text{max}} = 72.6$

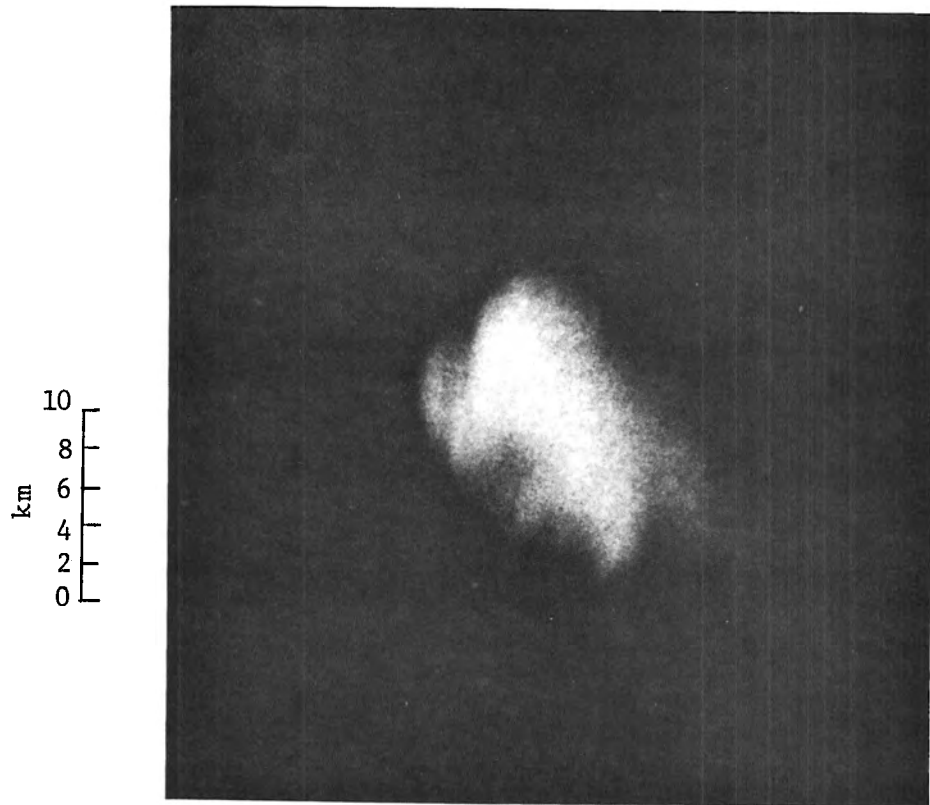


Figure 5.5g.
20:32:10 MDT
Elevation Angle
 $10 \log Z_{\max} = 71.8$

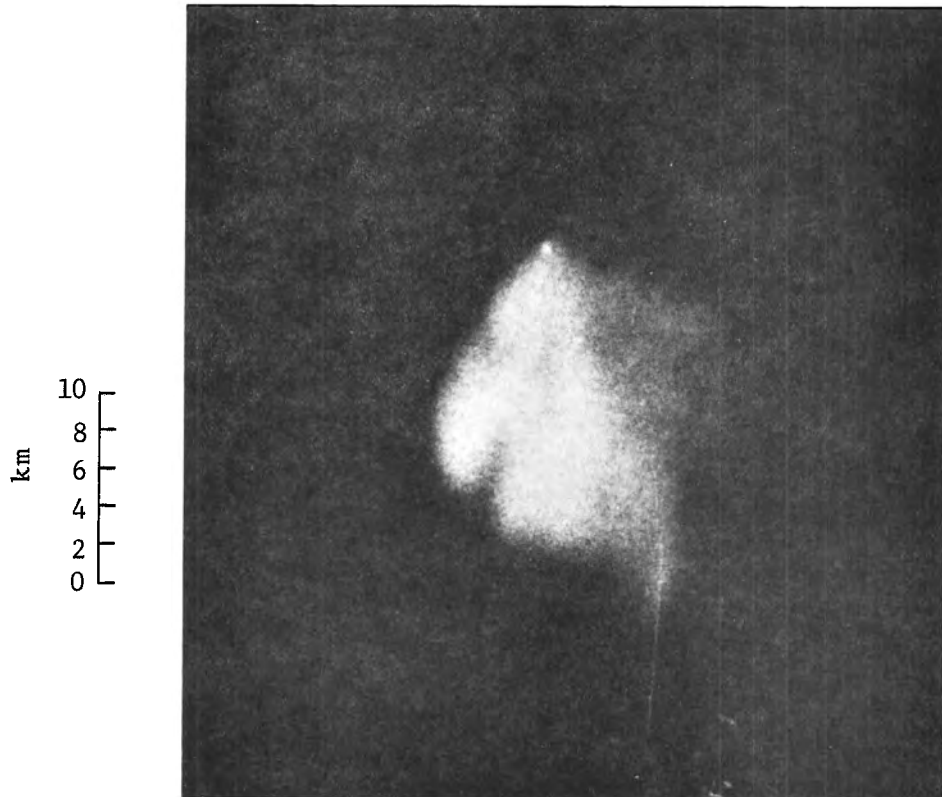


Figure 5.5h.
21:42:00 MDT
Elevation Angle 3.2°
 $10 \text{ Log } Z_{\text{max}} = 60.7$

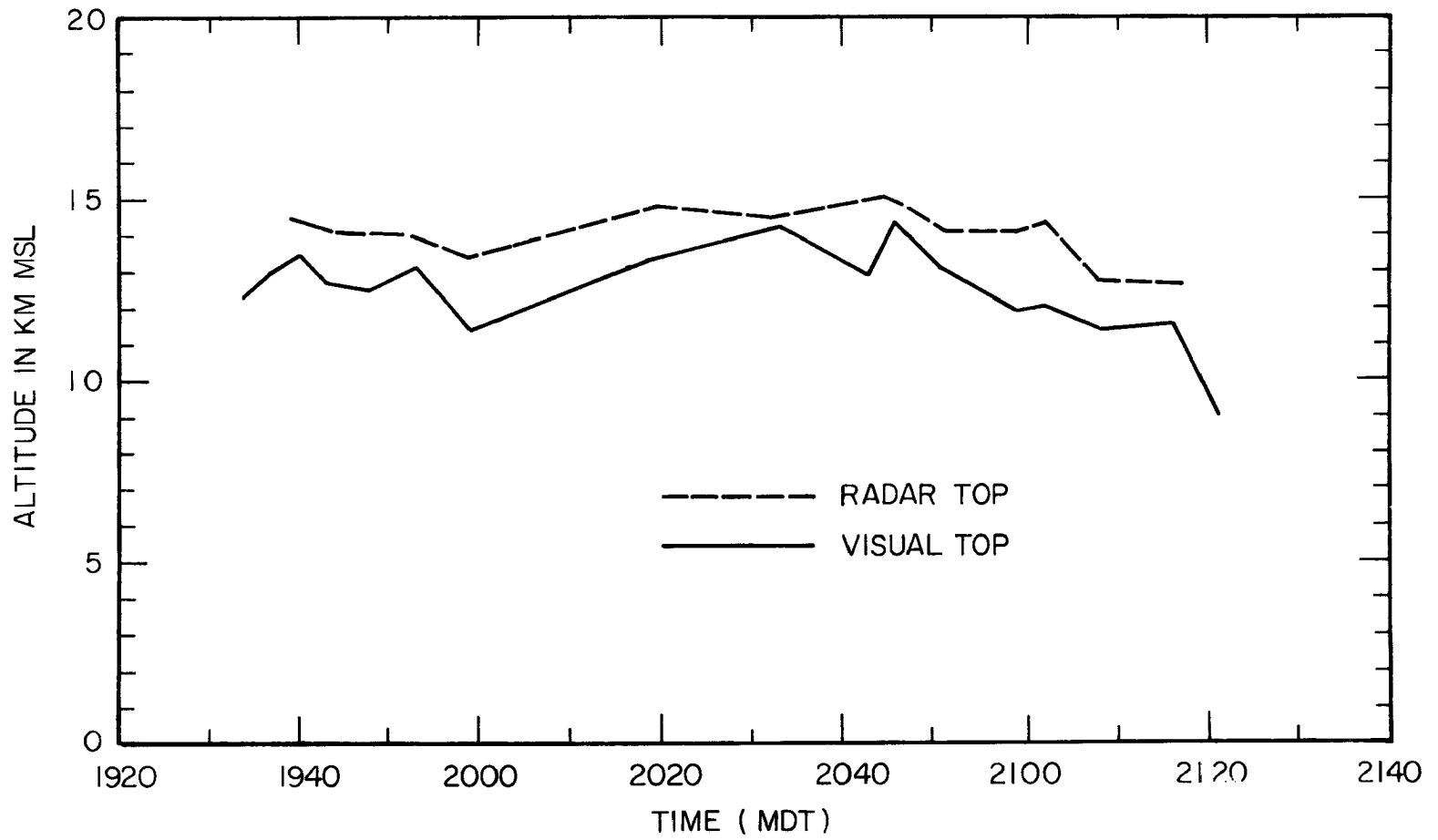


Figure 5.6. 34 mm radar and visual tops of the hailstorm of 28 July 1968.

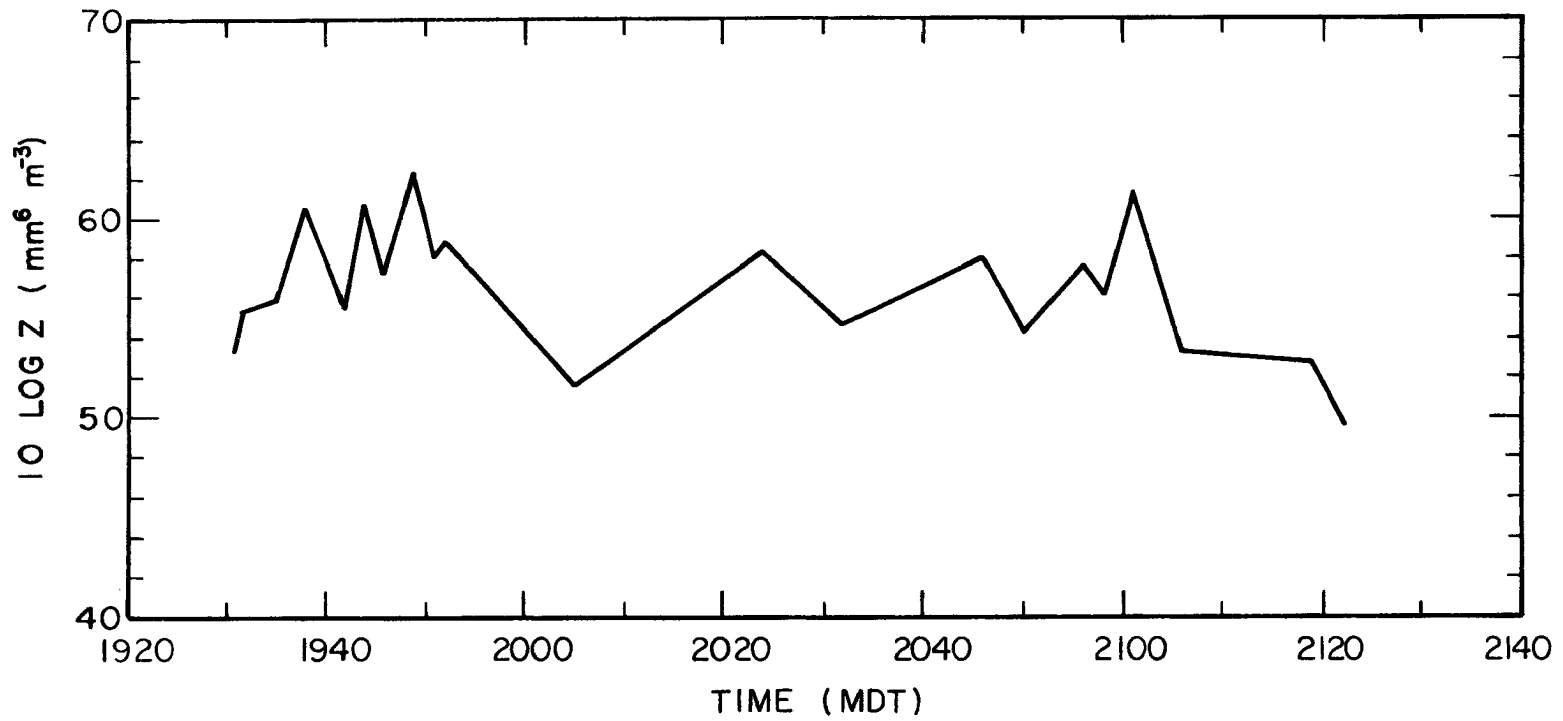


Figure 5.7. Maximum observed 34 mm reflectivity of the hailstorm of 28 July 1968. No correction for attenuation was made.

RHI Measurements

A series of 88 mm RHI photographs was taken beginning at 2035 MDT, shortly after the storm reached maximum intensity. These photographs are presented in Figure 5.8. The RHI sections are oriented approximately normal to the direction of motion of the storm with west being to the left. Figure 5.8a shows a well-defined vertical wall on the west side of the storm. A vertical 34 mm reflectivity scan was made in the zone of highest reflectivity as observed on this radar. The maximum observed 34 mm reflectivity was found to be near the edge of the wall. Reflectivity data were extracted from the 88 mm RHI photographs to agree in distance with the 34 mm data. The 88 mm data were increased 1.8 dB to account for the decrease in reflectivity of the storm in the 3 minutes between the 88 and 34 mm RHI records. Figure 5.9 shows vertical profiles of 88 and 34 mm reflectivity located approximately 0.5 km from the edge of the wall. Also shown is a vertical profile of the difference between the reflectivities.

The observed reflectivity difference varied from 8 to 9 dB between altitudes of 5 and 10 km. The difference was smallest at an altitude of 2 km where it was 3 1/2 dB. This two-wavelength vertical reflectivity profile was located to the northwest of the hail reports. Considering monodisperse wet hail between the freezing level and the -20°C isotherm (8 km), and a 3 dB uncertainty in the reflectivity measurements, an observed difference of 8 1/2 dB would indicate hail of 11-14 or 46-50 mm diameter. Figure 5.9 shows that the reflectivity difference decreases at altitudes below 6 km. If the hailstones were initially of 46 to 50 mm diameter in the supercooled water droplet zone, the reflectivity difference should not decrease as the stones melt as they fall to the surface. Sulakvelidze et al. (1965) has developed equations and nomographs for calculating hailstone melt during free fall. Using the observed mean temperature lapse rate of $7.1^{\circ}\text{C km}^{-1}$ at 2000 MDT and a 3.4 km distance between the heights of the freezing level and the ground, one finds that a hailstone initially 48 mm in diameter above the freezing level would melt to a final diameter of 45 mm by the time it reaches the ground. According to Figure 2.2, the reflectivity difference should increase by 4 dB, from an initial value of 10 dB to a final value of 14 dB, during this

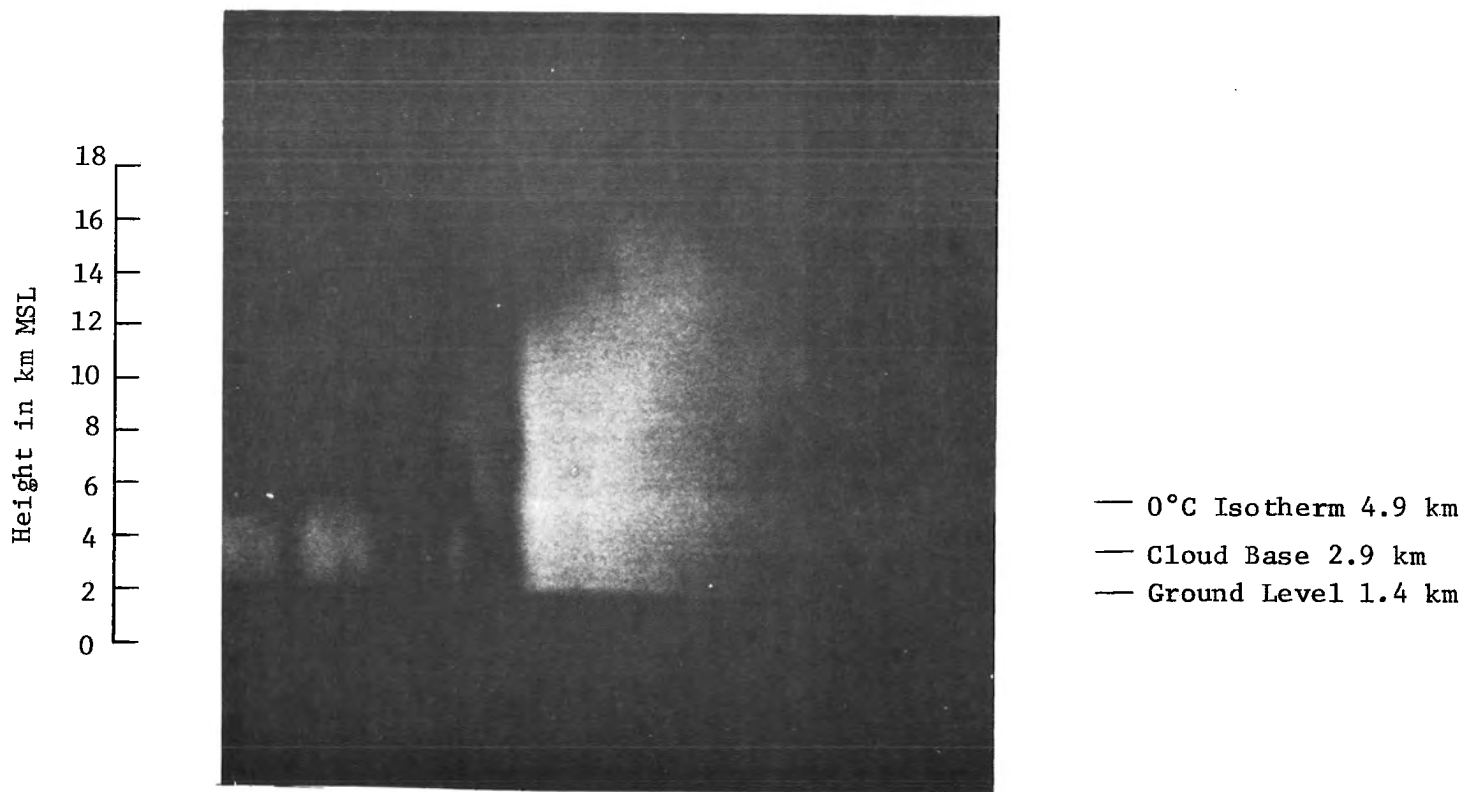
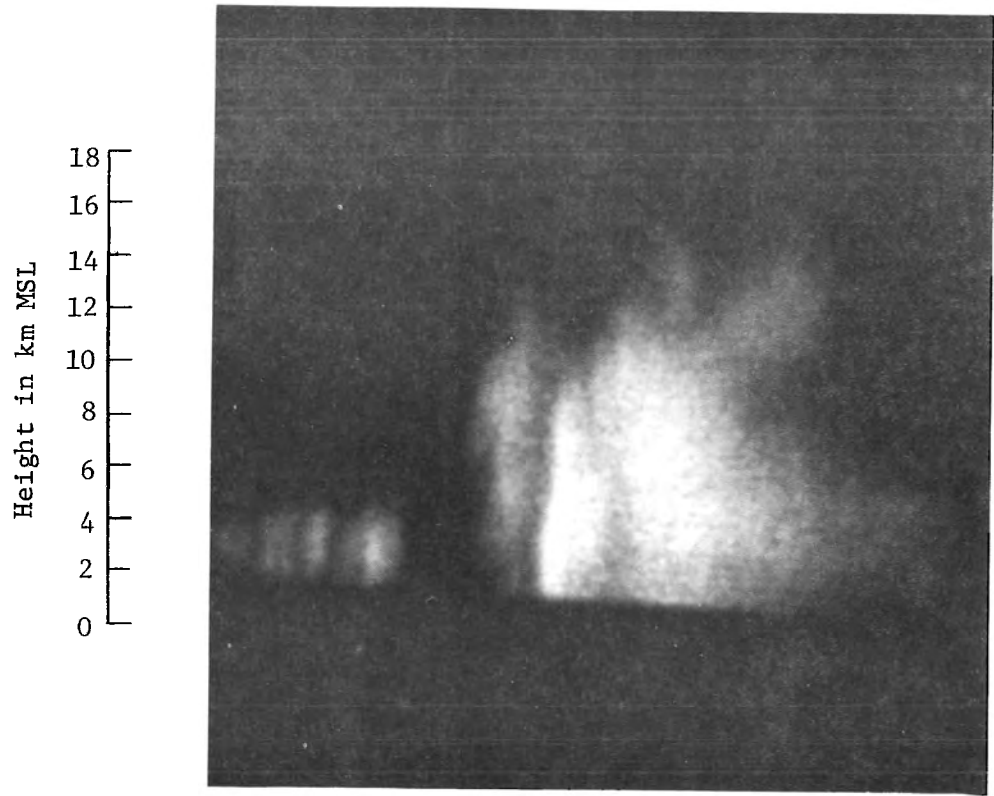


Figure 5.8a.
20:35:00 MDT
Azimuth 099.5°

Figure 5.8. 88 mm RHI photographs of the hailstorm of 28 July 1968, shortly after it reached maximum intensity. West is to the left. Scale: 1 cm 2.8 km. The vertical scale equals the horizontal scale.



- 0°C Isotherm 4.9 km
- Cloud Base 2.9 km
- Ground Level 1.4 km

Figure 5.8b.
20:35:30 MDT
Azimuth 101.5°

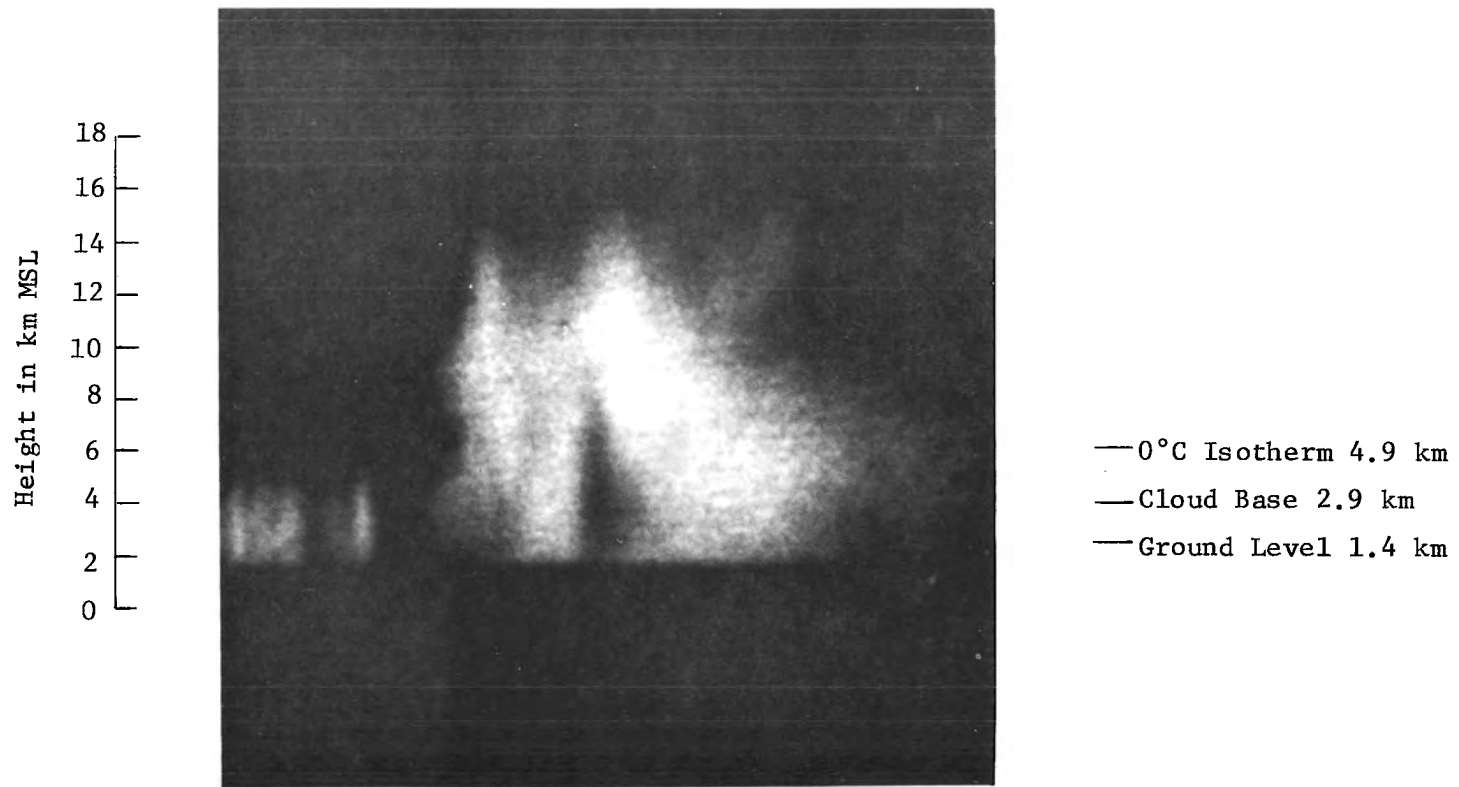


Figure 5.8c.
20:36:00 MDT
Azimuth 103.5°

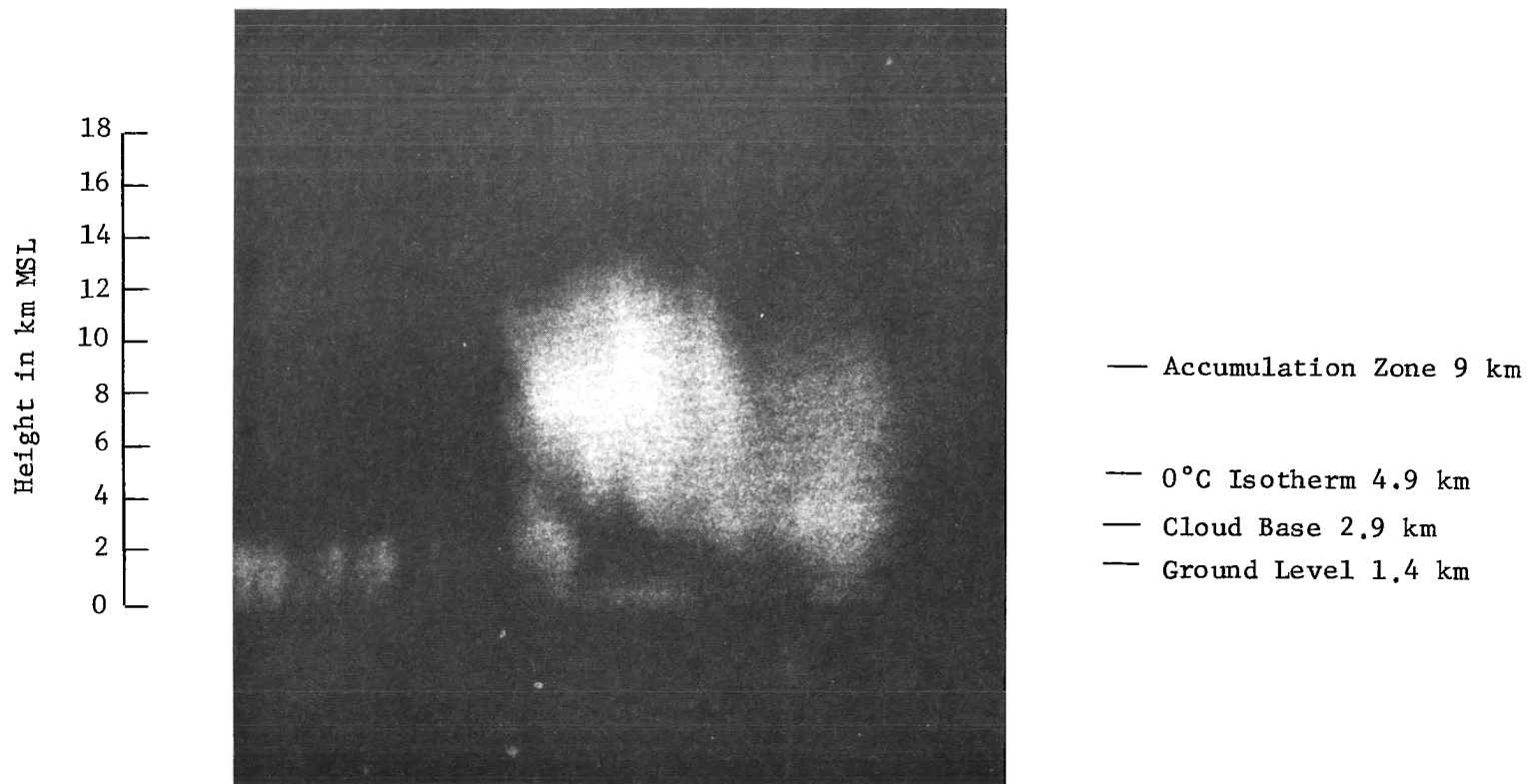


Figure 5.8d.
20:36:50 MDT
Azimuth 105.5°

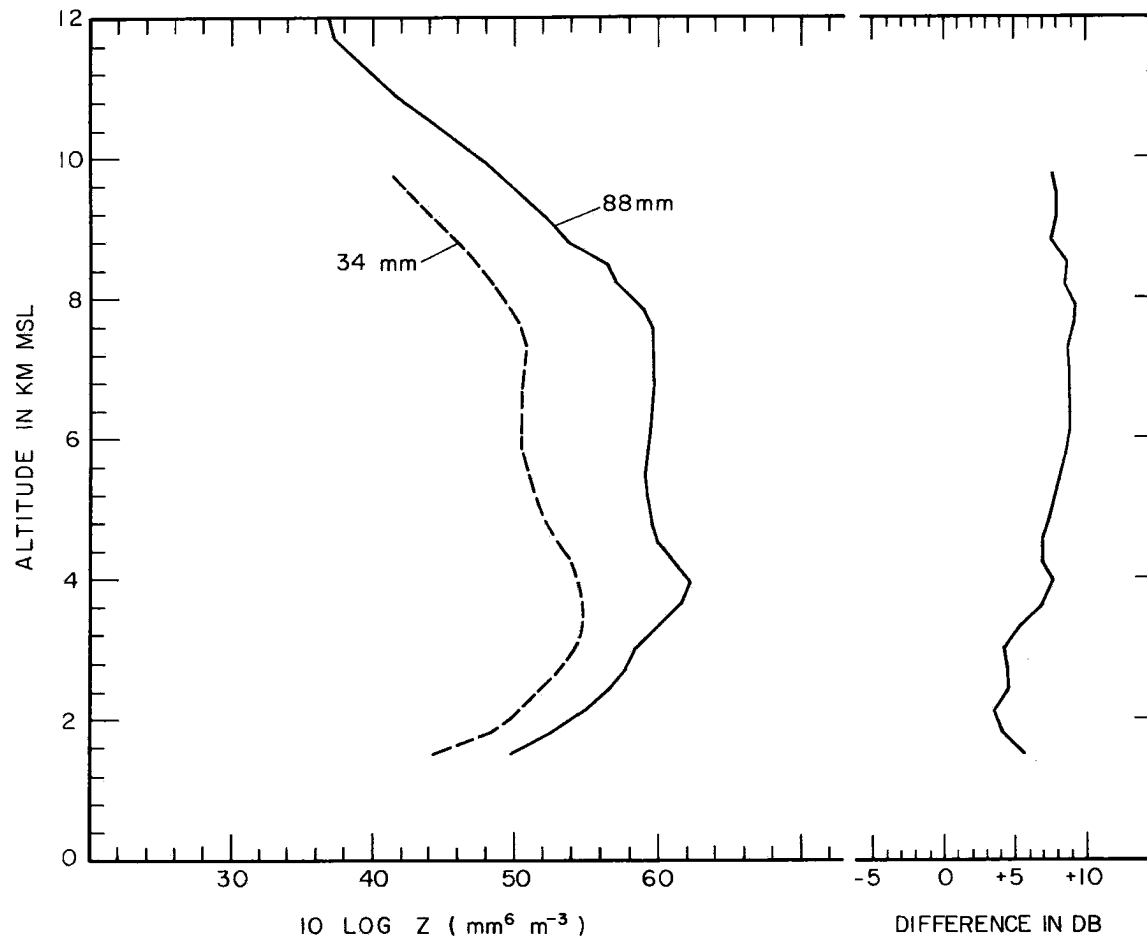


Figure 5.9. Reflectivities vs. height for 88 and 34 mm radar waves observed on 28 July 1968 at 2032 MDT at the distance of maximum 34 mm echo. The reflectivities are not corrected for attenuation
Azimuth: 100.13° Range: 69.6 km

process. Hailstones initially 14 mm in diameter would melt to 5 mm diameter by reaching the ground, and the reflectivity difference would change from 8 1/2 dB at the freezing level to -4 dB at the ground level during the melting. Hailstones of less than 12 mm diameter at the freezing level would melt completely before reaching the ground. Figure 5.9 shows that the reflectivity difference at 2 km altitude is about 3 1/2 dB lower than that at the freezing level. This would lead one to believe that the hailstones were initially between 11 and 14 mm diameter. Figure 5.8a shows that the radar echo reaches the ground in the area where the reflectivity measurements were taken, about 0.5 km in from the wall on the western flank of the storm. Heavy precipitation from a cumulonimbus appears as a solid echo all the way to the ground. Much of this precipitation was probably in the form of rain. Some farmers in this area reported as much as 1.5 inches of rainfall from this storm. The 3 1/2 dB decrease in the reflectivity difference is considerably less than what is predicted by theory. It may be possible that a heavy concentration of large (2-3 mm diameter) raindrops masked much of the change in reflectivity difference expected during hailstone melt. Due to the heavy precipitation occurring when the photograph was taken, the reflectivity maximum is at a relatively low height, 4 km.

If exponential hail size spectra are considered, the problem of finding the hail size becomes more difficult, as is mentioned in Chapter II. For the case of wet hail where the parameter Λ is unknown, the observed 8 1/2 dB difference above the freezing level corresponds to hailstones of 13 to 23 mm diameter. If one uses $\Lambda = 0.3$ as proposed by Douglas (1964), the predicted size range would be 15-23 mm. A 3 dB error in measurement is again assumed. Figure 2.6 shows that as the hailstones melt, decreases in the reflectivity difference would be observed, provided that most of the stones in the spectrum are initially of a size that would decrease appreciably during free-fall melting. From the analysis of the dual wavelength reflectivity data assuming monodisperse and exponential size spectra, it is concluded that the hail was probably about 15 mm in diameter (grape size). This hail would not be very large by the time it reached the ground. Unfortunately, no ground reports were available in the immediate vicinity

of the area where the reflectivity measurements were made. The main hailswath does appear to be located to the east, however.

At an azimuth of 100.13° the absolute reflectivity maxima, 67.3 at 88 mm and 54.6 at 34 mm, occurred at different distances, 72.5 and 69.6 km for 88 and 34 mm wavelengths respectively. This 2.9 km difference was caused by attenuation of the 34 mm radar waves by cloud and precipitation particles. This attenuation made it nearly impossible to determine the 34 mm reflectivity in the central core of the storm. One is able to observe only the outer fringes of well-developed thunderstorms with this wavelength.

This storm fitted the model of Browning and Ludlam (1962) in that it moved to the right of the middle-level winds and had a well-defined wall with an echo-free region adjacent to it. This wall, shown to be straight up and down within the resolution of the radar (400 m) and to have a reflectivity gradient sharper than could be resolved by the radar, was arranged parallel to the direction of motion of the storm. The wall is shown in Figure 5.8a. A partially enclosed echo-free region was observed at 2015 (Figure 5.5e). A reflectivity "hole" is also shown in Figure 5.8c. Because of the lack of supporting PPI photographs of the storm at several elevation angles at the time this picture was taken, no definite conclusions can be made as to whether or not this hole is, in fact, a vault. Figure 5.8d shows what appears to be an accumulation zone located in the reflectivity "nose" of the storm. The maximum reflectivity in Figure 5.8d is located at an altitude of about 9 km MSL.

Discussion

While the dual-wavelength detection system concept appears worthy of further study, some difficulties have been found in using the dual-wavelength radar data in the detection of discrete hailstone sizes. For example, it has become apparent that one cannot simply use the maximum observed reflectivities in any part of the storm. Strong attenuation of the 34 mm energy causes the 34 mm reflectivity maximum to occur in a different part of the storm than the 88 mm maximum. In this case study, the difference in distance was about 3 km. At 2024

MDT the 34 mm maximum was 4 km nearer the radars. At the distance of the 34 mm maximum at this time, the 88 mm reflectivity was clearly 16 dB less than its maximum.

At the distance of the 34 mm maximum, the 88 mm reflectivity often had a steep gradient making it difficult to measure the difference in reflectivity. The distance of the two measurements must be the same requiring careful comparison of the delays, pulse lengths and video responses. In the 88 mm radar the pulse is 400 m long. Although the distance circuits of the two radars were measured when calibrating them with a sphere, one cannot be sure that this is adequate. For a strong reflectivity gradient choice of distance will affect the result. For example, for a 16 dB km^{-1} gradient an error of 200 m in measuring the distance results in a 3 dB error in the reflectivity. A major operational problem was the lack of electronic synchronization of the radar antennas. In addition, the 88 and 34 mm radars had different beamwidths, 1.69° and 1.13° , making it impossible to compare reflectivities in precisely the same cloud volume. Also, the two radar constants are each not known better than 2 dB. Furthermore, because of the additional questions of the particle shape and distribution, one consequently encounters difficulty in inferring hail size from reflectivity measurements at 88 and 34 mm wavelengths.

However, initial growth of wet hail in convective clouds should be observable using the 88 and 34 mm radars. In early stages of the storm, attenuation of 34 mm radiation may not be an intractable problem because of the lower particle concentrations. Initial growth was not observed in the storm studied because it had already reached a mature stage when radar observations began. No other well-documented cases were available for study. The ability to detect the initial growth of hail in convective clouds, using radar as a passive sensing device, is of utmost importance to the success of hailstorm modification experiments. During the summer of 1969, the effectiveness of seeding potential hailstorms with aircraft-fired rockets will be evaluated. For the seeding to be most effective, the rockets must be fired into the accumulation zone at the time when the hailstones are just beginning to grow. Proper timing is critical since it is

believed that the hail growth, once it starts, proceeds rapidly, and a few minutes delay may result in little or no reduction in the hail size by seeding.

The ability to detect the initial hailstone growth is therefore extremely important to the timing and placement of the rocket nucleating payloads. The use of longer radar wavelengths and electronically synchronized radar antenna scanning is desirable in the observation of hailstorm development and evaluation of seeding effects. As mentioned in Chapter II, the use of longer wavelength radars, such as 230 and 88 mm wavelengths, enables one to measure larger hail sizes than is possible with the 88 and 34 mm combination (Figure 2.4). It is important to know if a storm is already well-developed, since the seeding of a mature storm may have little effect on the distribution of hail size reaching the ground. More importantly, attenuation is negligible at long wavelengths, and reflectivities in the core of a storm can be accurately measured with both radars. This is of critical importance in evaluating seeding effects where measurements in the accumulation zone are required. Some storms may be intense enough, even in early stages, to render X-band reflectivity data unusable due to attenuation. Electronic synchronization of the radar beams will result in a more efficient radar operation, with an increase in both the quantity and quality of radar data.

Chapter VI

CONCLUDING REMARKS

A severe hailstorm has been studied in detail with 88 and 34 mm wavelength radars with the objective of evaluating the usefulness of two-wavelength radar in detecting hail and hail growth in convective clouds. The storm selected for study was already in a mature stage when radar observations began, and no data on the initial stages were available. The Russian operational methods in hail suppression involve finding an accumulation zone when the storm is in a growing stage and where the hail is not yet large. The method used on this storm was to find the maximum 34 mm reflectivity and make two-wavelength reflectivity measurements at that location. The results of this study indicate that using two-wavelength radar to estimate hail size in a well-developed storm is unfeasible because the 34 mm radiation is strongly attenuated by cloud and precipitation particles. These findings differ from those of Atlas and Ludlam (1961) and Sulakvelidze et al. (1965) in which hail sizes in fully developed storms were measured using multi-wavelength radars. It has been shown in Chapter V that attenuation of short wavelength radiation is a serious problem which cannot be neglected. Reliable estimates of the amount of attenuation cannot be obtained without full knowledge of the composition, concentration and size distribution of the intervening particles. Some other problems involved are the unknown shape and distribution of the hailstones, errors in the reflectivity measurements, and lack of electronic antenna synchronization. In the calculations presented in this paper, the hailstones have been assumed to be spherical. It has been shown from scattering theory that it is not possible to accurately measure the size of large monodisperse hail because of the oscillatory nature of the scattering functions. Finding the size of large hail in an exponential spectrum is not possible since adding a few large particles to the distribution does not change the reflectivity difference.

The VGI group has claimed that the hail as measured at the ground is within 35 per cent of the size calculated from their radar measurements, after correction for melting during free fall. More accurate

measurements of the larger sizes are not likely because of the limitations imposed by scattering theory and the ever-present uncertainty in the accuracy of radar reflectivity measurements.

It has been shown in this paper that initial growth of monodisperse wet hail should be observable with the 88 and 34 mm radars. Growth of exponentially distributed hail should also be observed, but with less precision. If the hail is wet and monodispersely distributed, one may be able to use two long-wavelength radars to measure the size, as shown in Figure 2.4. Attenuation is not a problem here, since it is minimal at both wavelengths.

Recommendations for further research

Future studies should involve efforts to actually observe initial hail growth in convective clouds. Although attenuation of 34 mm radar waves is inescapable, it may not be a severe handicap during the growing stages of a hailstorm where the radar echo is relatively small and the particle concentrations are relatively low. The ability to detect initial growth of hailstones is of prime importance to the success of hail modification experiments, which, in the near future, will involve seeding the supercooled water droplet region of the clouds with aircraft-fired rockets. It appears the clouds must be seeded before the hail grows too large, in order to obtain any benefits of reduced hail size. The existence of the accumulation zone, as proposed in the VGI hailstorm model, should be verified. An attempt should be made to determine in a broad sense how the hailstones are distributed in the accumulation and precipitation zones.

Successful studies of hailstorm structure and dynamics will require well-coordinated efforts of all personnel involved. Some characteristics of hailstorms that merit further study are the accumulation zone and its relation to the updraft profile, the so-called "vault" as described by Browning and other investigators, and natural time variations in hailstorm reflectivity and their relation to the general structure of the storm. Knowledge of the location of the accumulation zone with respect to the updraft profile will be of importance in cloud seeding experiments, since the operators

must know precisely where the seeding material is to be injected. A number of investigators have proposed that the vault is a region of very strong updrafts and low particle concentrations. Further studies of the vault region by both radar and aircraft will yield valuable information about the general structure and dynamics of hailstorms. The study of natural time variations of reflectivity in hailstorms will be of importance when the results of cloud seeding must be evaluated.

REFERENCES

- Aden, A. L., 1952: Backscattering of electromagnetic waves from spheres and spherical shells, Geophysical Research Paper No. 15, Geophysics Research Division, U. S. Air Force Cambridge Research Center, Cambridge, Mass., 42 pp.
- Atlas, D., 1965: Activities in radar meteorology, cloud physics, and weather modification in the Soviet Union, Bulletin of the American Meteorological Society, 47, 696-706.
- Atlas, D., W. G. Harper, F. H. Ludlam and W. G. Macklin, 1960: Radar scatter by large hail, Quarterly Journal of the Royal Meteorological Society, 86, 468-482.
- Atlas, D. and F. H. Ludlam, 1961: Multi-wavelength radar reflectivity of hailstorms, Quarterly Journal of the Royal Meteorological Society, 87, 523-534.
- Battan, L. J., 1959: Radar meteorology, University of Chicago Press, Chicago, 161 pp.
- Bent, A. E., 1946: Radar detection of precipitation, Journal of Meteorology, 3, 78-84.
- Born, M. and E. Wolf, 1965: Principles of Optics, Pergamon Press, New York, 808 pp.
- Browning, K. A., 1965: The evolution of tornadic storms, Journal of the Atmospheric Sciences, 22, 664-668.
- Browning, K. A., J. Hallet, T. W. Harrold and D. Johnson, 1968: The collection and analysis of freshly fallen hailstones, Journal of Applied Meteorology, 7, 603-612.
- Browning, K. A. and F. H. Ludlam, 1962: Airflow in convective storms, Quarterly Journal of the Royal Meteorological Society, 88, 117-135.
- Bushnell, R. H., 1967, Personal communication.
- Deirmendijian, D. and R. J. Clasen, 1962: Light Scattering on Partially Absorbing Homogeneous Spheres of Finite Size, The Rand Corporation, Santa Monica, Report No. R-393-PR, 44 pp.
- Donaldson, R. J., 1958: Analysis of severe convective storms observed by radar, Journal of Meteorology, 15, 44-50.
- Donaldson, R. J., 1959: Analysis of severe convective storms observed by radar-II, Journal of Meteorology, 16, 281-287.

- Donaldson, R. J., 1961: Radar reflectivity profiles in thunderstorms, Journal of Meteorology, 18, 292-305.
- Donaldson, R. J., 1965: Methods for identifying severe storms by radar: a guide and bibliography, Bulletin of the American Meteorological Society, 46, 174-193.
- Donaldson, R. J., A. C. Chmela and C. R. Shackford, 1960: Some behavior patterns of New England hailstorms, Geophysical Monographs No. 5, Physics of Precipitation, American Geophysical Union, Washington, 354-368.
- Douglas, R. H., 1960: Observations of Alberta hailstorms, Cumulus Dynamics, Proceedings of the First Conference on Cumulus Convection, C. E. Anderson, ed., Pergamon Press, New York, 145-147.
- Douglas, R. H., 1963: Recent hail research, Meteorological Monographs, 5, no. 27, Severe Local Storms, American Meteorological Society, Boston, 157-167.
- Douglas, R. H., 1964: Hail size distributions, Proceedings of the 1964 World Conference on Radio Meteorology, American Meteorological Society, Boston, 146-149.
- Douglas, R. H. and W. Hitschfeld, 1959: Patterns of hailstorms in Alberta, Quarterly Journal of the Royal Meteorological Society, 85, 105-119.
- Geotis, S. G., 1963: Some radar measurements of hailstorms, Journal of Applied Meteorology, 2, 270-275.
- Goyer, G., 1967: Hail Suppression in the U. S. S. R., Facilities for Atmospheric Research, No. 4, 17-21.
- Gunn, K. L. S. and J. S. Marshall, 1958: The distribution with size of aggregate snowflakes, Journal of Meteorology, 15, 452-461.
- Herman, B. M. and L. J. Battan, 1961a: Calculation of Mie backscattering of microwaves from ice spheres, Quarterly Journal of the Royal Meteorological Society, 87, 223-230.
- Herman, B. M. and L. J. Battan, 1961b: Calculation of Mie backscattering from melting ice spheres, Journal of Meteorology, 18, 468-478.
- Hitschfeld, W. and R. H. Douglas, 1961: A theory of hail growth based on radar and surface studies of Alberta storms, Proceedings of the Ninth Weather Radar Conference, American Meteorological Society, Boston, 153-158.

- Inman, R. L. and J. E. Arnold, 1961: Thunderstorm characteristics, Chapter II of Utilization of AN/CPS-9 Radar in Weather Analysis and Forecasting, Final Report, Contract AF 19(604)-6136, Texas Agricultural and Mechanical University, College Station, Texas, 8-73.
- Kerr, D. E., ed., 1951: Propagation of Short Radio Waves, Vol. 13, Massachusetts Institute of Technology Radiation Laboratory Series, McGraw-Hill, New York, 728 pp.
- Kotov, N. F., 1960: Radiolokatsionnye kharakteristiki livnei i groz. (Radar characteristics of showers and thunderstorms.) Leningrad. Glavnaia Geofizicheskaiia Observatoriia, Trudy, No. 102, 62-93.
- Marshall, J. S. and W. McK. Palmer, 1948: The distribution of raindrops with size, Journal of Meteorology, 5, 165-166.
- Mie, G., 1908: Beitrage zur Optik truber Medien, speziell kolloidaler Metallosungen, Annalen der Physik, 25, 377-445.
- Modahl, A. C., 1969: The influence of vertical wind shear on hailstorm development and structure. M. S. Thesis, Atmospheric Science Paper No. 137, Department of Atmospheric Science, Colorado State University, Fort Collins, Colorado, 55 pp.
- Pell, J., 1966: Quantitative hailstorm studies using a broad, vertical-beam radar, Proceedings of the Twelfth Weather Radar Conference, American Meteorological Society, Boston, 421-425.
- Renné, D. S., 1969: Stability and Dynamic Processes in the Formation of High Plains Hailstorms, M. S. Thesis, Atmospheric Science Paper No. 136, Department of Atmospheric Science, Colorado State University, Fort Collins, Colorado, 53 pp.
- Salomonson, V. V., 1968: Anisotropy in Reflected Solar Radiation, Ph.D. Thesis, Atmospheric Science Paper No. 128, Department of Atmospheric Science, Colorado State University, Fort Collins, Colorado, 143 pp.
- Schleusner, R. P. and A. H. Auer, Jr., 1964: Hailstorms in the high plains, Final Report, NSF Grant G-23706, Civil Engineering Section, Colorado State University, Fort Collins, Colorado, 100 pp., CER64RAS36.
- Shifrin, K. S., 1951: Rasseyaniye Sveta v Mutnoy Srede. (Scattering of Light in a Turbid Medium) Gosudarstvennoye Izdatel'stvo Tekhniko-Teoreticheskoy Literatury, Moscow. NASA Technical Translation, NASA TT F-477, Washington, D. C., 1968, National Aeronautics and Space Administration, 212 pp.

- Stephens, J. J., 1961: Radar cross-sections for water and ice spheres, Journal of Meteorology, 18, 348-359.
- Sulakvelidze, G. K., 1966: Rezul'taty rabot kavazskoi protivogradovoi ekspeditsii 1965. (Results of the Caucasus Anti-Hail Expedition of 1965.) Vysokogornyi geofizicheskii institut (Georgian High Mountain Geophysical Institute), Trudy, issue 7, 1-61, National Center for Atmospheric Research Library Translation No. 182, 1967.
- Sulakvelidze, G. K., 1967: Shower precipitation and hail, Gidrometeoizdat, Leningrad, 412 pp.
- Sulakvelidze, G. K., N. Sh. Bibilashvili and V. F. Lapcheva, 1965: Obrazovanie osadkov i vozdeistvie na gradovye protsessy. (Formation of precipitation and modification of hail processes.) Gidrometeorologicheskoe Izdatel'stvo, Leningrad. Translated from Russian, Israel Program for Scientific Translations, Jerusalem, 1967, 208 pp.
- United States Department of Commerce, ESSA Daily Weather Maps, Weekly Series: July 22-28, 1968, U. S. Government Printing Office, Washington, D. C.
- Visher, S. S., 1954: Climatic Atlas of the United States, Harvard University Press, Cambridge, Massachusetts, 403 pp.
- Ward, N. B., K. E. Wilk and W. C. Herrman, 1965: WSR-57 reflectivity measurements and hail observations, National Severe Storms Laboratory, Technical Note 3-NSSL-24, Washington, D. C., 1-8.
- Wilk, K. E., 1961: Radar reflectivity observations of Illinois thunderstorms, Proceedings of the Ninth Weather Radar Conference, American Meteorological Society, Boston, 127-132.